J. Fluid Mech. (1990), *vol.* 214, *pp.* 287–320.
Printed in Great Britain

An explanation for the multivalued heat transport found experimentally for convection in a porous medium

By C. R. B. LISTER
School of Oceanography, WB-10, University of Washington, Seattle, WA 98195, USA

(Received 18 April 1988 and in revised form 17 October 1989)

Convection experiments were conducted in a porous slab 3 m in diameter and 30 cm thick, using two quite different media: a filling of rubberized curled coconut fibre and of clear polymethylmethacrylate beads. The second experiment involved the successful use of a visualization scheme for the flows at the upper boundary. Convection began in a hexagonal pattern with a slight tendency to form into rolls, but became very complex, irregular and three-dimensional at higher Rayleigh numbers, without developing any obvious temporal instabilities. Above a Rayleigh number of 1000 a significant number of dendritic downwellings appeared, where smaller downwellings seemed to feed into larger areas such that the whole complex may have converged into a single downwelling plume. The visualization provides direct confirmation that the lateral scale of the convection decreases with increasing Rayleigh number, approximately as $(\mathscr{A}+C)^{-0.5}$.

Nusselt number versus Rayleigh number curves were obtained for both experiments. The only feature they have in common is a central section where the slope on a log/log graph is slightly over 0.5. On the graph from the first experiment, this section is preceded by a slope close to 1 and followed by a slope close to 0.33. The temperature measured at a point in the fill 25 mm below the top boundary was unsteady at conditions representative of the upper two segments of the graph; sensitivity was insufficient to measure fluctuations at lower temperature differences. The Nusselt number for the bead fill jumps upward just above onset (where $\mathscr{A} = 4\pi^2$), rapidly settles to a slope of 0.52, and then gradually breaks upward again to a slope of greater than 1. Increases in conductivity and permeability close to the boundary are not a large enough fraction of the boundary-layer thickness to cause this. A new phenomenon, lateral thermal dispersion, appears to be responsible. It occurs because there is no constant separation distance between adjacent channels in a bead fill. Thermal exchange in the junction pores exceeds the average if the flow is fast enough, especially when the fluid is more conductive than the beads.

A simple boundary-conduction theory can be matched to the uncontaminated results. It is based on relative scaling of the residence time of fluid in the boundary layer, and predicts Nusselt number growth as the 0.55 power of Rayleigh number toward the high values typical of major geothermal areas.

1. Introduction

1.1. *Nusselt numbers of geothermal systems*

The key feature of a major geothermal system, whether on land or beneath the sea floor, is a high intrinsic heat transport. For example, pre-exploitation surveys at

Wairakei (New Zealand) measured a surface heat loss that summed to about 400 MW, mostly concentrated over a hot area of about 2 km^2 (Fisher 1964). Deep drilling at the nearby Broadlands area delineated a double plume of area less than 2 km^2 at a depth of 1 km, confirming that the spreading of thermal phenomena at the surface tends to be due to the mushrooming of the upwelling plume (Grindley & Browne 1975; Elder 1965). These data are quite rudimentary, but nevertheless allow the estimation of one of the two primary dimensionless numbers of any convective system. The Nusselt number is simply the ratio of the thermal flux transported by convection to the flux that would be transported by conduction alone. Given the natural convective flux and the area of hot phenomena, one only needs to estimate the depth and temperature of a plausible heat source, apply a factor of 2 to 4 to the area to include recharge, and a Nusselt number can be calculated. Microearthquakes were observed at a depth of 7 km beneath the Rejkanes (Iceland) geothermal area (Ward 1972), so that it seems reasonable to fix a source of 500 °C at 5 km. The conductive flux is therefore 0.3 W/m^2 and the advective flux over 6 km^2 is 70 W/m^2, leading to a Nusselt number of 230.

1.2. *Nusselt numbers and boundary layers*

Without any further knowledge about the convective system, a high Nusselt number N can be related to the formation of boundary layers. At an impervious boundary, all the heat must be transported by conduction. At a microporous open boundary, this is still true (Ribando, Torrance & Turcotte 1976), but fails when macroscopic plumes erupt through the boundary, such as at the sea-floor smokers (Corliss *et al.* 1979). The mean thermal gradient at the boundary must be N times the overall thermal gradient across the convecting medium, so that the mean-temperature profile in a porous convecting slab must look like figure 1. The boundary-layer thickness can therefore be conveniently defined as $h/2N$, where h is the height of the slab. The deviation from this of a natural effusive boundary is not material: even there, a system circulating meteoric water must acquire its heat at a hot impervious boundary at depth, where the boundary layer develops. It is interesting that, even when such a large natural system is given a generous heat-source area of 6 km^2, the boundary-layer thickness is only 11 m.

1.3. *Laboratory experiments*

The importance of this becomes clear when experimental work on porous convection is examined. The purpose of laboratory work is not to directly simulate a natural geothermal system, but to obtain an understanding of the mechanics of the convection, such as the pattern and aspect ratio of the convecting cells and, in particular, of the effect of the instability, or Rayleigh number. For a porous slab, the Rayleigh number is defined as

$$\mathscr{R} = \frac{\alpha_{\mathrm{L}} g D h \Delta T}{\kappa \nu_{\mathrm{L}}}, \tag{1.1}$$

where α_{L} is the expansion coefficient of the fluid, g is gravity, D is permeability, ΔT is the temperature difference, κ is a diffusivity found by dividing the matrix thermal conductivity k by the heat capacity of the fluid and ν_{L} is the kinematic viscosity of the fluid (Wooding 1957). Where properties vary with depth and temperature, appropriate averages can be taken (e.g. Straus & Schubert 1977). Convection begins above a critical Rayleigh number of $4\pi^2$ (Lapwood 1948), as has been verified by Hartline & Lister (1977) in a Hele-Shaw cell (Hele-Shaw 1898). The Nusselt number is identically unity below the critical Rayleigh number for a horizontal slab, and

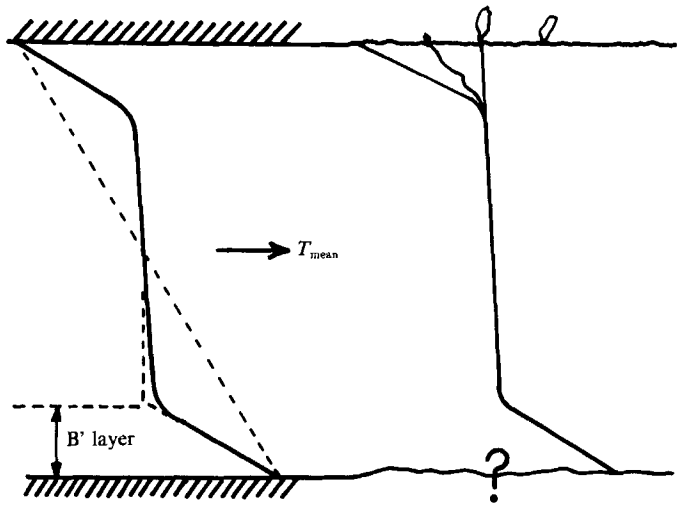

FIGURE 1. Left: a plot of horizontally averaged temperature T(mean) against depth for an idealized convecting porous slab (solid line). In the absence of convection, the conductive temperature profile would be as given by the dashed line. At the boundary, where heat must be transferred by conduction, the gradient must be N times steeper, where N is the convective Nusselt number. A convenient definition of the boundary-layer thickness is therefore $h/2N$, where h = slab thickness. Right: varying upper profiles in a real geothermal area, due to the variation of permeability near the surface. Nothing is actually known about the basal boundary, though the water penetration theory (Lister 1974) predicts a boundary very similar to the idealized one of an infinitely conducting heat sink.

differs negligibly from unity even when there is topography on the conductive boundaries (Hartline 1978). Above the critical Rayleigh number convection begins abruptly, with cells whose aspect ratio is robust to wavy topography on boundaries and even advection of the medium, at least for two-dimensional systems (Hartline & Lister 1981; Fehn & Cathles 1979).

One would expect there to be some general relation between Rayleigh number and Nusselt number, subject to relatively minor variations caused by other dimensionless numbers. For example, the heat transport of free convection between parallel conducting plates has been shown to be a weak function of the Prandtl number ν/κ (Rossby 1969). If there *were* such a general relation, it would be possible to estimate the Rayleigh number, and hence the deep permeability of natural systems, as well as produce reasonably accurate models for their formation and evolution (e.g. Lister 1974, 1984). Instead, a compilation of some of the published data on heat transport demonstrates a wide variation over a limited range of moderate Rayleigh numbers (figure 2). A feature of many of the experimental curves is a sudden breakover from a slope of near 1 to a slope of about 1/3. This was attributed by Elder (1967) to a change from porous-medium convection to a form of free convection. The breakover was supposed to occur when the Nusselt number for porous convection, growing linearly with increasing temperature difference, overtook the Nusselt number for free convection of the same fluid, growing according to a fractional power law. The idea was that the presence of the 'obstacles' can hardly increase the heat transport over that of free fluid, which should certainly be true if the beads or matrix have a similar thermal conductivity to that of the fluid. Problems arise in applying this criterion when the matrix is much more or much less conductive than the fluid, and in any case it gives little insight into the physics of the mechanism.

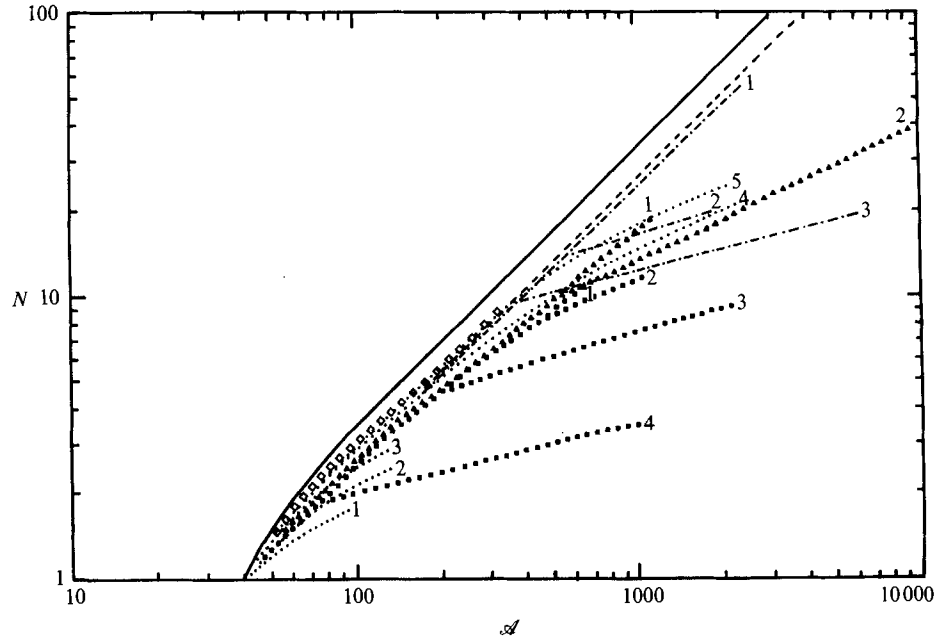

FIGURE 2. A representative compilation of published heat transport data, rescaled where necessary to show onset close to the theoretical critical Rayleigh number of $4\pi^2$ (Lapwood 1948). This value for the onset has been confirmed by a sensitive experiment in a Hele-Shaw cell (Hartline & Lister 1977); some published results differ owing to problems in measuring the physical properties of heterogeneous media. ——, A theoretical upper bound to the heat transport obtained with a variational method by Busse & Joseph (1972); their two-wavenumber solution takes off more steeply at a Rayleigh number of 280. – – –, Hele-Shaw cell, thickness 4.75 mm, oil; 3, 5, 8 mm glass beads; 6 mm plastic balls; heights and configurations not given, except that the last, high-Rayleigh-number experiment was like an overgrown coffee percolator filled with foam plastic beads and water (Elder 1965). –·–·–, 1 = 'granular material'; 2 = 8 mm glass spheres; 3 = 18 mm glass spheres, no other data. A Hele-Shaw cell, height 2 cm, width 30 cm and thickness 6 mm, kerosene fill, followed curve 1 up to a Rayleigh number of 800 (Elder 1967). · · · · ·, 1 = 1.9 mm quartz sand, water; 2 = 2.25 mm quartz sand, water and 4 mm lead balls, water; 3 = 1.9 mm quartz sand, oil; 4 = 1.7, 3.0, 4.0 mm glass beads, water; 5 = 0.9, 2.0 mm glass beads, oil and 4 mm polypropylene spheres, water; all depths 5.35 cm (Combarnous 1970). ◇◇◇, 3.25, 5.25 mm glass beads, water and 5.25 mm glass beads, silicone oil, no other data (Bories 1970). ■■■, 1 = 1 mm to 7 mm glass beads, water; 2 = 10 mm glass beads, water; 3 = 10 mm glass beads, turpentine; 4 = 15 mm steel balls, turpentine; height 4 cm (Schneider 1963). ▲▲▲, 1 = 3 mm glass beads, water, depth 4.3 cm and 6 mm glass beads, depth 8.6 cm; 2 = 14.3 mm glass beads, water, depth 8.8 cm (Buretta & Berman 1976). In these last three cases, the symbols are used only to make curves visibly separate: they are not data points.

A close examination of figure 2 shows no obvious systematic relation between the conditions of the experiments and the levels of the curves, a situation not helped by offhand reporting of experimental details. The confusion has led to two other suggestions of what influences the breakover in slope: that there is some sort of 'finite' heat transfer coefficient between fluid and solid, or that there is a fundamental change in the convection to a 'fluctuating regime' (Combarnous & Bories 1975; Caltagirone, Cloupeau & Combarnous 1971). All of these suggestions can in fact be combined into one elegant and simple criterion: the convection changes to a form of free convection when the boundary-layer thickness defined above comes comparable with the pore size of the porous medium. An unusually accurate experiment in a liquid has shown that the power law for heat transport in free convection is close to

1/3 (Katsaros *et al.* 1977), and Krishnamurti (1970*b*) has shown that the high-Rayleigh-number regime is turbulent. Some of the additional apparent scatter in figure 2 is due to the difficulty of making corrections for the variation of fluid properties with temperature, and of measuring the true matrix properties in the first place. If published data had to be rescaled in Rayleigh number to show a common onset of convection at the value $4\pi^2$, then it is likely that the Nusselt numbers are also in error. It will later be argued that the very high Nusselt numbers reported by Elder are due to lateral thermal dispersion in his apparatus. This phenomenon leads to a still more-stringent criterion for a bead-type fill to model a porous medium.

1.4. *Size of apparatus*

A critical parameter for porous slabs is the ratio of slab height to pore separation, since this limits the maximum Nusselt number that can be attained before the boundary layer ceases to span several pores. A high Nusselt number requires also a high Rayleigh number, and so the permeability of the bed needs to be high. However, it is well known (e.g. Scheidegger 1974) that the permeability of a bed of beads is proportional to the square of the bead size, so that large beads are required to achieve a high permeability. This means that the slab height must be large, and it is also desirable to maintain a large aspect ratio. Otherwise transitions in the size of convective cells are liable to be sudden (as in Hartline & Lister 1981) and this will cause cusps to form in the Nusselt-number curve (e.g. Combarnous & Bories 1974). Thus, a very large apparatus is needed to investigate this problem properly.

2. The apparatus

A fibreglass tank was constructed capable of holding a porous layer 30 cm thick and circulators for the hot and cold boundaries 7 cm thick. The shape, dictated by the use of a double-spiral of aluminium channel for the hot base, was an irregular hexagon 3 m across the flats (figure 3). Insulation 15 cm thick on base and sides was estimated to have a thermal leakage (dry) of 1.2 and 0.6 W/°C respectively. Heat was provided by a heater system distributed throughout the spiral and controlled by duty-cycle switching through a range of 1 W to 33 KW. Feedback of the product of current and voltage assured maintenance of the nominal 1% power accuracy from 10 W upwards, and the zero offset was calibrated by timing the power pulses with a stopwatch. The circulating pump used for the second experiment had a provision for measuring the mechanical heat input.

The cooling circulator was in the form of a swirlpool fed by a central and six tangential jets, graded in volume to reduce radial temperature gradients (see figure 10). Lake water was added to the flow of a recirculating pump to maintain the jet water at a constant temperature; the return flow temperature was measured as most representative of the boundary temperature and rose a maximum of 1 °C above the jet temperature for the highest thermal flux.

A schematic section through the apparatus is shown in figure 4, as configured for the second experiment. Long, averaging temperature sensors had been perfected by then, so that it was possible to measure a temperature representative of that of the metal boundary as well as that of the hot circulator water. The bottom sensor was calibrated by replacing the swirlpool with a layer of insulation and heating the whole apparatus. Leakage was too great to obtain a reliable calibration of the mid-fill sensor, so that its resistance coefficient was assumed the same as that of the bottom one.

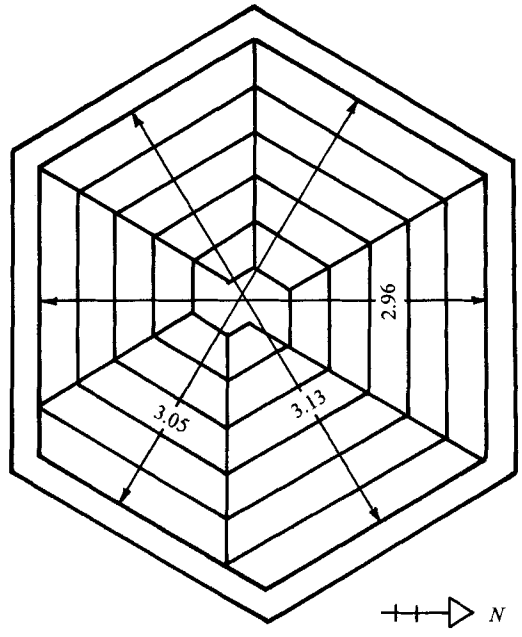

FIGURE 3. Diagram of the dimensions of the apparatus (in m), also showing the double-spiral construction of the hot circulator. The outer rim is insulation up to the level of the porous fill, and a channel for the recirculating water above that. The fill is 30 cm thick, giving an aspect ratio of 10:1 (after Gibson 1980).

The temperature drop between the circulating fluid (mercury-in-glass thermometer) and the bottom averaging sensor is shown in figure 5. The slope of less than 1 is characteristic of forced convection aided by thermal convection. Discussion about the use of these data is given in the text pertaining to figure 8.

3. Experiment 1: fibre packing

3.1. *Experimental techniques*

In the search for materials of small pore size and high permeability, it was thought that an ideal had been found in rubberized curled coconut fibre, a product used for filters and packaging. The grade chosen had fibres about 3 mm apart, and had a stable flat shape, so that the apparatus would be filled precisely by 12 layers of the material. A labyrinth was constructed to provide enough path length to measure the permeability, and the results are shown in figure 6. The scatter at the low-velocity end is due to the difficulty of measuring accurately a head difference of less than 1 mm; in the end, a measuring telescope was used to compare the heights of spar buoys made out of sewing needles, cork and paint. The apparent slight increase in permeability with velocity is heavily dependent on the single high-velocity point, but it is what would be expected for the drag of a fibre tangle: as the Reynolds number rises, the effective drag cross-section of each fibre declines, leading to less obstruction of the flow. The Reynolds number of 2 corresponds to the flow velocity of a plume at the Rayleigh number of about 2200, using the measurements of Hartline (1978) in a Hele-Shaw cell. The permeability has shown only a small change up to this point, and the flow is not locally turbulent because the Reynolds number for flow around

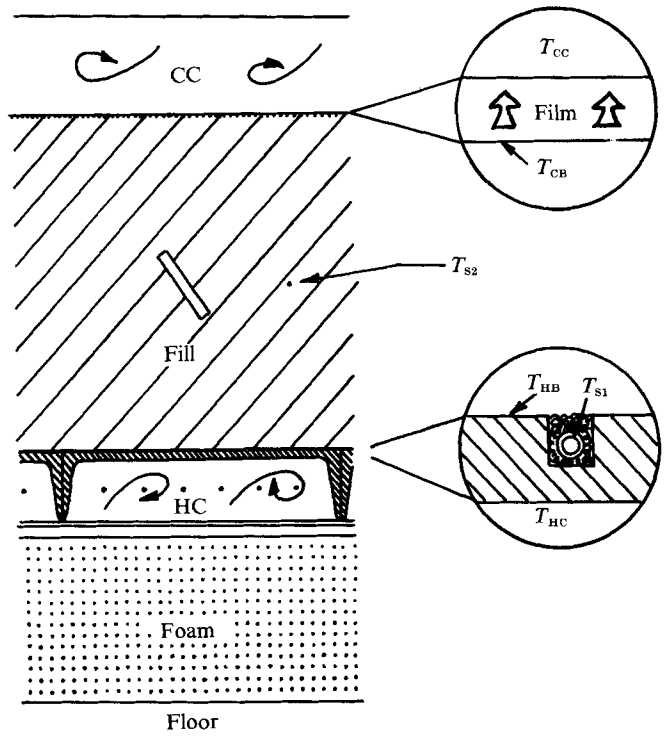

FIGURE 4. Schematic cross-section through the apparatus, configured as for the second experiment. Scale is given by the 30 cm thickness of the fill. HC = hot circulator, T_{HC} = temperature thereof, dots = heating cables, T_{HB} = true boundary temperature, T_{S1} = temperature measured by long cylindrical sensor grouted into groove, T_{S2} = temperature measured by similar sensor in centre of fill, canted rectangle = section through graphite anode, T_{CB} = temperature of cold boundary, dotted zone beneath this = stainless-steel cloth cathode, T_{CC} = temperature of cold circulator, CC = swirl pool of cold circulator. It will be apparent that T_{S1} may be lower than T_{HB}, and that the difference between T_{CB} and T_{CC} is the sum of the drop across the clear plastic film and a drop similar to that between T_{HC} and T_{HB}. The first experiment had an aluminium top plate, no visualization scheme, and no usable internal sensors other than some silicon diodes 2.5 cm below the top boundary.

each fibre remains well below unity at all temperature differences achieved by the apparatus.

The near 100% porosity of the curled fibre has the advantage that the remaining properties of the medium are effectively those for pure water, and therefore well known. However, the ease with which water convects is a strong function of temperature, and some correction scheme must be devised to account for this. Figure 7 presents logarithmic plots of the variation with temperature of the relevant properties of water. The Nusselt number, a function of $1/k$, can be obtained very simply in the corrected form

$$N = \frac{W(1-(T_m-20-0.2\mathscr{T})\,0.0028)}{(T_{HC}-T_{CC}-\mathscr{T})\,15.9}, \tag{3.1}$$

where W = heater input; $T_m = 0.5\,(T_{HC}+T_{CC})$, the mean temperature; 0.0028 is the slope of $1/k$ variation against temperature; T_{HC} = hot circulator temperature;

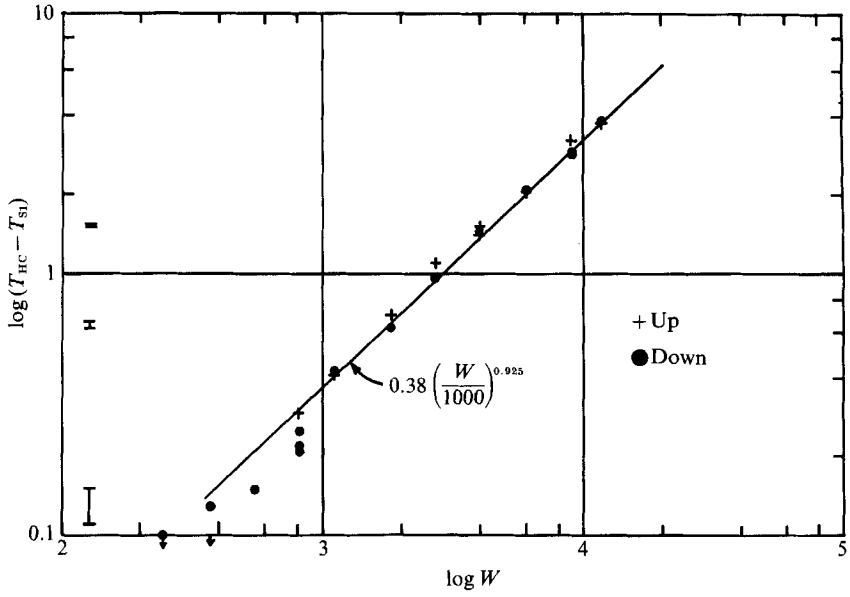

FIGURE 5. Plot of the temperature difference between the hot circulator water and that measured by a long cylindrical sensor grouted into a groove on the upper surface of the aluminium hot boundary, against input power W in W. Error bars at the left indicate the expected size of the temperature error. The equation of the fitted line is only a guide to the temperature drop between fluid and metal, because the sensor groove was not closed in by a conductive metal cap (see figure 4).

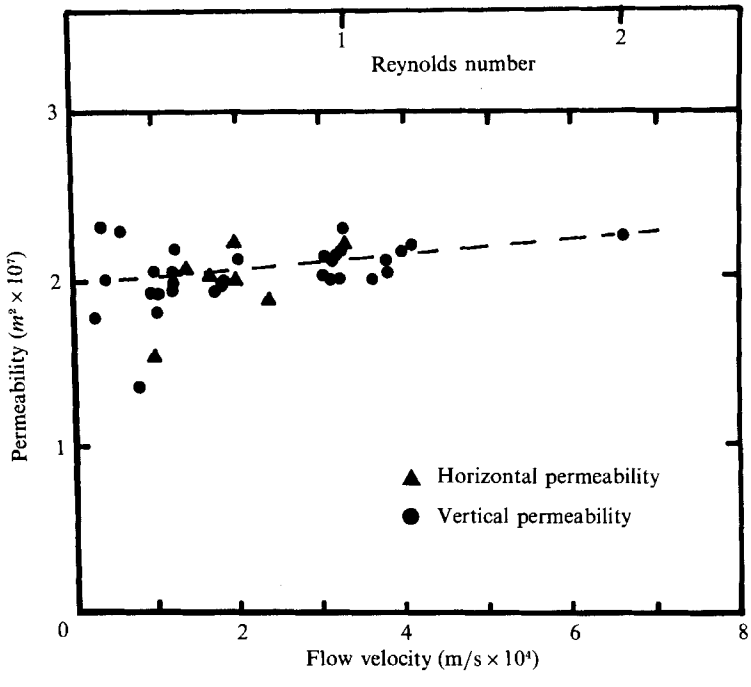

FIGURE 6. Permeability of rubberized curled fibre batting, versus flow velocity. Reynolds number is based on a 3 mm fibre-to-fibre spacing. The dashed line, indicating a slight increase with velocity, is heavily dependent on the single high-velocity point. However, an increase with increasing Reynolds number is expected; the Reynolds number of 2 corresponds to the porous plume velocity at a Rayleigh number of 2200 (see text) (diagram after Gibson 1980).

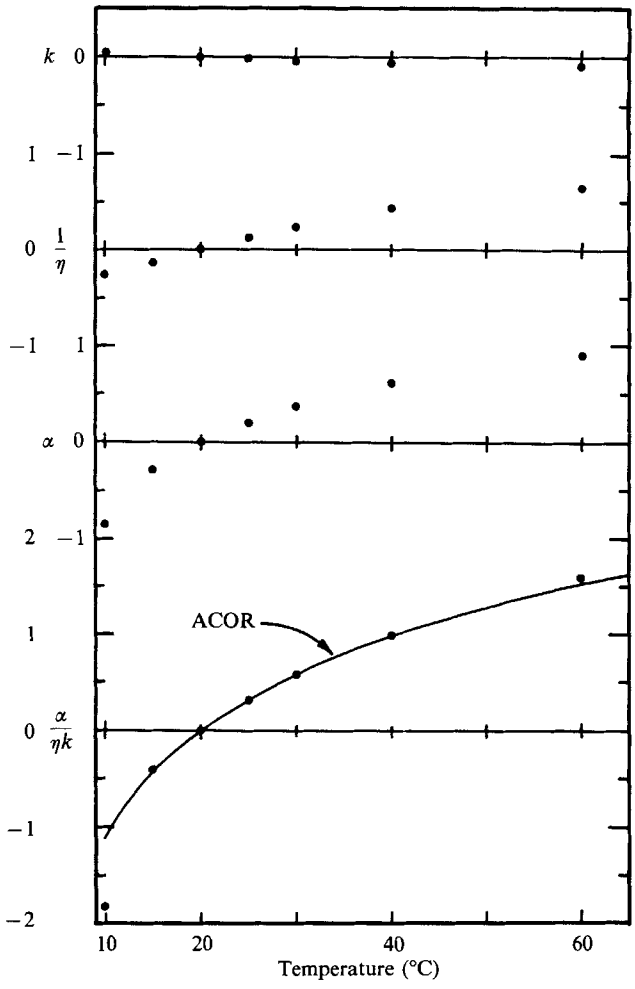

FIGURE 7. Plots of the properties of water influencing the convection, expressed as natural logarithms of the ratio to the properties at 20 °C. k = thermal conductivity; η = dynamic viscosity; α = expansion coefficient. The bottom graph shows the combined effect of these property changes on the calculation of Rayleigh number, and a quadratic fit to the central region called ACOR (see text).

T_{CC} = cold circulator temperature; 15.9 = the known heat conductivity of a slab of water 30 cm thick and 8.14 m^2 in area; and

$$\mathscr{T} = 0.41\left(\frac{W}{1000}\right)^{0.925}, \tag{3.2}$$

is the corrected estimate of the sum of the temperature drops between both circulating fluids and their respective boundaries (see discussion below). A small fraction of this is subtracted from the mean temperature to allow for the fact that the top boundary is expected to have a thinner fluid boundary layer than the bottom boundary, as the cold circulator pump power is nearly 100 times greater than that of the hot circulator.

The properties of water that determine the Rayleigh number (equation (1.1)) are

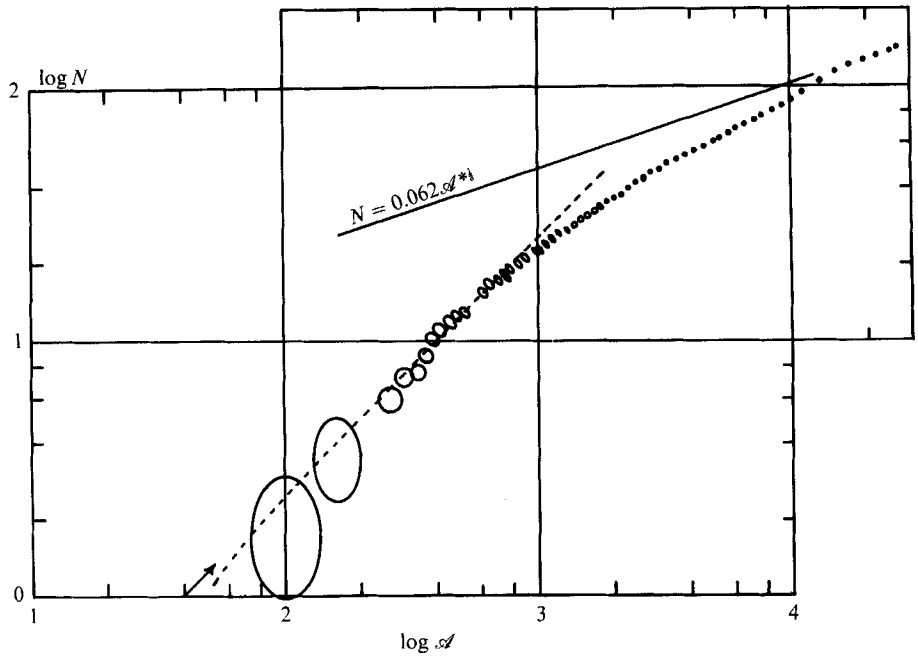

FIGURE 8. Quantitative results of the first experiment, expressed as logarithmic plot of Nusselt number against Rayleigh number. Error ellipses represent estimates of the precision of the points. The straight line with a slope of 1/3 represents the theoretical heat transport of free convection according to Katsaros *et al.* (1977) and Howard (1966). The dashed curve is a plot of equation (5.4) from the discussion section (see text).

combined at the bottom of figure 7 and, between 15 °C and 40 °C, are fitted by a quadratic called

$$\mathrm{ACOR} = (1+(T-20)\,0.072+(T-20)^2\,0.0005), \tag{3.3}$$

giving a Rayleigh-number relation

$$\mathscr{A} = 916\,(T_{\mathrm{HC}}-T_{\mathrm{CC}}-\mathscr{T})\,(1+(T_{\mathrm{m}}-20-0.2\mathscr{T})\,0.072+(T_{\mathrm{m}}-20-0.2\mathscr{T})^2\,0.005) \tag{3.4}$$

that is corrected for changing water properties according to the mean temperature in the porous slab. The justification for this is in the results obtained by Booker (1976) for the heat transport of free convection with a fluid with a very strong temperature-dependent viscosity. Even though the hot plumes become much narrower than the cold plumes, a Nusselt number calculated using the Rayleigh number obtained from viscosity at the mean temperature is within 1% of the experimental data for a viscosity ratio of 4:1, and within 12% for a ratio of 300:1.

3.2. *Experimental results*

The results of the experiment are shown in figure 8. Except for the three lowest points, all data were obtained with decreasing power loads since air bubbles appeared under the top boundary on the way up, and interstitial air was probably impeding the flow. The very large error ellipses at the low-Rayleigh-number points are due to the very low fluxes and temperature differences near the onset of convection. The first point is taken at 2.5 W heater power, comparable to leakage fluxes and with an unknown (for this experiment) power contribution from the hot circulator pump; the

measured temperature difference is only 0.10 °C, so that the disagreement between the data and the theoretical onset is not significant.

The most obvious feature of the curve is the gradual change in slope from near 1 at low Rayleigh number to near 1/3 at high Rayleigh number. Superimposition of a transparent copy of figure 8 over figure 2 shows that the Nusselt number is nearly coincident with the upper bound of the experimental data (and below the upper theoretical bound) in the mid-Rayleigh-number range, and then drops below the curves of Elder (1965, 1967) as the slope flattens. In this respect the result does not differ qualitatively from the older data except for the density of points and the gradualness of the change. Quantitatively, however, the Nusselt number approaches that due to free convection through a slab of the same geometry, calculating a free-convection Rayleigh number by the relation

$$\mathscr{A}^* = 4.047 \times 10^8 (T_{\mathrm{HC}} - T_{\mathrm{CC}} - \mathscr{T})(1 + (T_{\mathrm{m}} - 20 - 0.2\mathscr{T})\,0.072 + (T_{\mathrm{m}} - 20 - 0.2\mathscr{T})^2\,0.0005), \quad (3.5)$$

and using the relation

$$N = 0.062\mathscr{A}^{*\frac{1}{3}} \quad (3.6)$$

of Katsaros *et al.* (1977). This result differs from that reported by Khurana (1988) for convection in helium, where it appears as if the slope of the Nusselt-number curve drops to 2/7 above a Nusselt number of 30. At a Rayleigh number of 10^9 the Nusselt numbers are: helium 79, water 62 from the two experiments. The Prandtl number ν/κ is an order-of-magnitude larger for water than for helium, and this could account for the differences in both Nusselt number and exponent. In the work of Rossby (1969) the trend was to higher Nusselt number with higher Prandtl number; here it seems to be reversed. Since there is almost as great a problem with measurement of free convection heat transport as there is in porous media, it is conservative to use the results of a careful experiment using the same fluid.

3.3. *Theoretical insights*

When the boundary layers become thinner than the spacing between the curled fibres, the peel-off mechanism should be little influenced by their presence, and the convection should be indistinguishable from free convection in the entire absence of the porous fill. This is a special property of the fibre-tangle type of fill with near 100 % porosity, and is not matched by other porous beds where the beads or particles interfere substantially with free convection. Another way of looking at this problem is the discussion in Ping Cheng (1978) where, in media of 'very high' permeability the effective Rayleigh number changes from $\mathscr{A}^*$ to $\mathscr{A}^* D/h^2 = \mathscr{A}$ as D/h^2 goes from 0.1 to 0.01. This represents the change from flow dominated by fluid/fluid friction to fluid/bed friction, and it is implied that the onset of convection is being discussed. When boundary layers are well established, h should be replaced by the boundary-layer thickness, or perhaps that thickness multiplied by 27/20, since the critical Rayleigh number of a porous slab with one solid and one open boundary is 27 rather than 40/2 (Wooding 1957). Working back from the permeability, convection should be substantially that of a porous medium when $h = 4.5$ mm and substantially free when $h = 1.4$ mm. The respective boundary-layer thicknesses should therefore be 3.3 mm and 1.05 mm, or Nusselt numbers of 46 and 143.

Comparing these numbers to the curve in figure 8, the slope has already *changed* substantially by a Nusselt number of 46, but seems to have closely approached 1/3 by the highest Nusselt number achieved, 141. This justifies the fitting of the highest

measured point to the free convection Nusselt line by changing the numerical factor in figure 5 to that of equation (3.2). Increasing the factor moves measured points up to the left at a 45° angle, since the Nusselt number is increased and the Rayleigh number decreased when the effective temperature difference is reduced. Perhaps that last point should have been left a short distance below the free-convection Nusselt line; the kink in the curve outlined by the last 10 measurements makes it difficult to evaluate the approach to asymptotic slope. If so, the true correction factor should be somewhat smaller, but the qualitative features of the results remain the same, and the shift of the highest points in the second experiment would be comparable with the symbol size because of the lower power levels reached in that experiment.

It remains to note two things about this first experiment. One is that the Nusselt number/Rayleigh number slope has dropped below unity before the boundary layers should behave as if in free convection, so that there might be a fundamental change in the slope of the curve for a true porous medium. The other is that time-series temperature measurements at a silicon diode buried in the fill 25 mm below the top boundary showed fluctuations at all Rayleigh numbers tried down to 2580 ($N = 44$), which was the lowest for which temperature changes were measurable with the instrumentation used (digital sensitivity 0.05 °C). This is above the first break in slope for the Nusselt-number curve, but the fact that a 'fluctuating regime' occurs here does not mean that it would for a porous medium of low or moderate porosity. The near 100% porosity of the curled fibre allows boundary layers to peel off just as in free convection; this is not possible in a low-porosity medium because the primary heat capacity there is in the stationary matrix, and convective patterns can change only slowly as heat is advected from one part of the matrix to another.

4. Experiment 2: Lucite beads

4.1. *Characteristics of the porous material*

It was clear after the first experiment that the porosity, particularly the thermal porosity equalling the fraction of advectable heat capacity after allowing for dispersion, is an important dimensionless number for porous-medium convection. It is not practical to reach values as low as in a cracked rock (5% or less), as the permeability would then be too low for a useful laboratory experiment, but it should be low enough to stabilize the convective patterns until boundary layers become thinner than the pore size. A commercially available polymethylmethacrylate ('Lucite' T.M.) bead was selected for the fill as it is clear, cheap and has a low thermal conductivity. Manufactured as a feedstock for plastic moulding, the beads are not round but slightly rounded short cylinders of 3 mm diameter and length. The sharp edges might induce turbulence into the channel flows earlier than for rounded beads. An experiment on the permeability of pea gravel had shown that there was about a 20% permeability loss at a pore-velocity Reynolds number of 200, based on mean particle diameter. Using the Hele-Shaw cell velocity data of Hartline (1978), this Reynolds number should be reached in the apparatus at a Rayleigh number of 300000, more than 100 times the highest actually achieved.

Alternatively, one can test for the validity of Darcy's linear law (Darcy 1856), using the discussion in Ping Cheng (1978) whereby the Reynolds number should be less than about 0.1, when based on flux velocity and $D^{\frac{1}{2}}$ for lengthscale, for a 5% deviation in the friction. Given that the permeability of the fill is 3.3×10^{-9} m^2 (see below), this more stringent condition requires the flux velocity to be less than 1.7 mm/s and the dimensionless velocity to be less than 1800, as scaled by κ/h for the

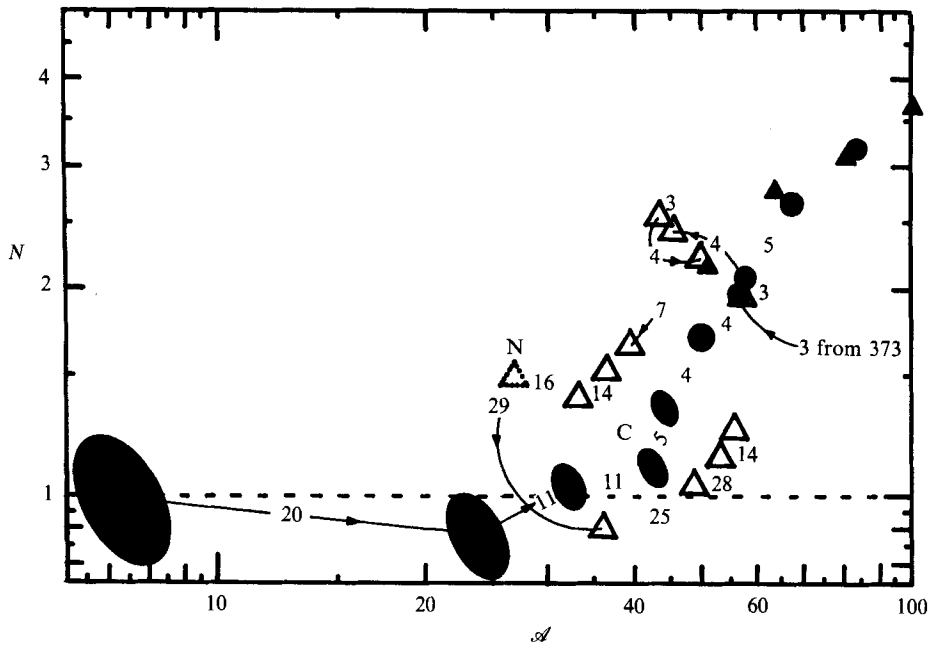

FIGURE 9. A plot of Nusselt number measurements against Rayleigh number near the onset of convection. The position of the scales on both axes has been set by examination of the sequence of solid elliptical or circular symbols, whose dimensions are an estimate of the errors. They were obtained during startup of the experiment when the insulation between apparatus and floor was dry and the conditions in the crawl-space beneath the building were believed stable. Solid triangles were obtained during the main decreasing-power series of measurements, as in figure 11, and open triangles were obtained after a final hot excursion to degas the fill. N indicates no convection detectable by the visualization scheme, while C indicates onset. Small numbers between the open triangles and the solid rounded symbols give the number of days of stabilization before measurement of the next point in the sequence (arrows where obscure). A small leak had reduced the quality of apparatus insulation during the acquisition of open-triangle data, and underfloor air circulation was more variable than before.

fill and its height. Again, using an extrapolated fit to the velocity data of Hartline (1978), this velocity should be reached at a Rayleigh number of 23000, comfortably above the highest values actually reached. Even the hot plumes, with their substantially lower viscosities (see figure 7) should experience an unchanged permeability.

The problem with an irregular bead fill is that the permeability and the thermal conductivity are both affected by the packing density. In particular, the packing achieved in the long columns of an apparatus to measure the permeability is not likely to be as dense as in the open bed of the big apparatus. It was decided to rely on a suggestion of J. R. Booker (personal communication) of using the apparatus itself to determine these quantities by studying the onset of convection. The filled circular or elliptical points in figure 9 show the upward progression in power levels when the apparatus was freshly filled. On the basis of this progression, it was felt that a Nusselt number of 1 could be chosen within 10% giving

$$N = \frac{W(1-(T_{S2}-20)\,0.0028)}{(T_{HC}-T_{CB}-\mathscr{T})\,7.65}, \tag{4.1}$$

which differs from (3.1) by having a measurement of the mean fill temperature T_{S2}

(see figure 4) replacing T_m, having a cold-boundary temperature T_{CB} corrected for the thermal drop across the boundary film, and in the numerical factor. This last implies that the conductivity of the matrix is 0.29 W/m °C, compared to that for pure water of 0.60 W/m °C and for polymethylmethacrylate of 0.17 W/m °C. This is not unreasonable for a mixture with porosity 0.38 and a structure with tortuosity to the paths through the higher conductivity material.

4.2. *Convective properties of the apparatus*

The same, consistent, upward progression of conditions was felt to establish the Rayleigh number within 5% as

$$\mathscr{A} = 30.1(T_{HC} - T_{CB} - \mathscr{T})(1 + (T_{S2} - 20)\,0.072 + (T_{S2} - 20)^2\,0.0005) \qquad (4.2)$$

by fitting various lines and curves to a figure scaled in the same general way as figure 9. As it was possible that sufficient stabilization time had not been allowed for this progression, an attempt was made at the end of the experiment (a full year later) to characterize the onset of convection more precisely. The result is the pattern of open triangles following the last excursion up to full power to degas the apparatus (figure 9). At first sight these seem to negate the supposed precision of the original determination of N and $\mathscr{A}$, and so a short discussion is needed.

The group of four open triangles with an upwards trend to the left at Nusselt numbers of 1.96 to 2.52 are the record for a deliberate attempt to see how long the convection took to restabilize after a sudden drop from a Rayleigh number of 373 ($N = 8.1$), the point indicated by the open triangle in figure 13. Conditions return closely to those before the excursion to degas the apparatus, but only after a substantial excursion and overshoot in the Nusselt number. Nevertheless, the flow patterns observed at the top boundary by the visualization scheme change only subtly over the 11 days between the first and last observations at a constant power input of 23.4 W. A 'time constant' of 31 hr is obtained by dividing the thermal resistance actually exhibited by the fill under these conditions (temperature drop near 1.4 °C) into the thermal mass of the hot circulator, 450 kg of water equivalent. This compares to fluid residence time in a plume of 13 hr, a plume re-equilibration time of 40 hr (assuming a 'thermal porosity' of about 1/3), a cell re-equilibration time of 6 days (four legs of a nearly square cell) and a thermal diffusion time for the slab by conduction of 15.5 days. The thermal mass of the hot circulator is therefore negligible compared with the times of convective pattern rearrangement, and the overshoot is likely to be due to the maintenance of plume velocities by heat stored in regions of matrix bathed by hot plume fluid, rather than by actual pattern rearrangement. Since the changes in the upward progression were small between stages, it is probable that enough time elapsed between the measurements except for the two 11-day periods prior to the actual onset of convection, denoted by the symbol C in figure 9.

There remains the problem of why the open triangles around the critical Rayleigh number display such a huge apparent hysteresis. The key is the dotted triangle of figure 9, labelled N to denote that the visualization scheme showed no fluid movement. Yet the Nusselt number appears to be 1.5 at an input power level of 8.6 W. A heat leak of only 3 W through the floor (3 °C across dry insulation, less across wet) would bring the dotted triangle of figure 9 down to a Nusselt number of 1. The existence of a reasonably stable point near the Rayleigh number of 7, where the only deliberate heat input was the hot circulator pump power of 1.6 W, shows

that the points around the critical flux of 8 W were reliable under the original conditions of cell startup.

The convective breakaway in heat transport, known to occur at a Rayleigh number of $4\pi^2$ (Lapwood 1948), and the conductivity estimated from the conductive heat transport, can be used to back-calculate a permeability. The value obtained is 3.3×10^{-9} m^2, and compares well with 4.4×10^{-9} m^2 calculated from the Kozeny formula

$$D = \tfrac{1}{5}P^3/S^2, \tag{4.3}$$

where P = the volumetric porosity and S = the surface area per unit volume, if one short cylindrical bead is assumed to be packed into every cube of the same 3 mm dimensions (Scheidegger 1974).

4.3. *Visualization of the flow*

The key feature of this experiment was to be a visualization scheme for the flow pattern. To this end, the metal top boundary used for the first experiment was replaced by a transparent Teflon film 0.18 mm thick. The maximum temperature drop across this film was 1.39 °C, while the corresponding drop across the porous fill, after all boundary corrections, was 35.0 °C. Beneath the film was a stainless-steel gauze of 40% opacity, and, buried halfway into the fill, were 13 graphite slabs, canted at about 45° to minimize their effect on the convection and heat transport (see figure 4). The plain water fill was changed to a solution of 27 p.p.m. bromothymol blue, acidified with both hydrochloric and acetic acids to be just to the acid side of the colour change from blue to yellow (pH about 5.5). The visualization operated when the stainless-steel gauze was made the cathode, and the graphite slabs the anode, for electrolysis by 60 V at 2 A for 10 min. The liquid near the cathode became more alkaline and changed to the blue form of the dye, a much more intense colour than the yellow. Flow caused the boundary fluid to migrate toward the downwellings and collect there before being removed into the bulk porous fill, where it mixed with fluid that had been made more acid at the anodes and disappeared. Numerous batches of coloured fluid could be made by this technique, the only cost being the gradual liberation of hydrogen and oxygen gases at the electrodes. The method was adapted from the report of Baker (1966) by the substitution of bromothymol blue for thymol blue, to bring the colour change closer to neutral pH. A search for and test of other dyes did not yield any superior to bromothymol blue.

The results, shown for various Rayleigh numbers in figures 10 and 11 in black and white, are the first visualizations of three-dimensional convection in a porous slab with two similar and normal boundaries. The only previous three-dimensional visualizations were the collection of fluid-phobic aluminium particles above the downwellings of a porous fill bounded on top by a thin layer of free fluid (Bories & Thirriot 1969) and observations of convection cells drifting through a small array of temperature sensors (Sondergeld & Turcotte 1977). The former experiment had a closed isothermal boundary on one side and a semi-open semi-insulated boundary on the other, while the latter lacked the resolution to do more than identify the existence of cells.

At a Rayleigh number of 50 convection was well-enough established to produce a clear pattern (figure 10*a*). Instead of the rolls universally expected for the initial form of convective breakdown, what is observed are hexagons spaced nearly two layer thicknesses apart. As the Rayleigh number was raised slowly from this point, the hexagons did seem to try to organize themselves into rolls. The asymmetry of the onset, whereby one boundary was maintained at constant temperature while

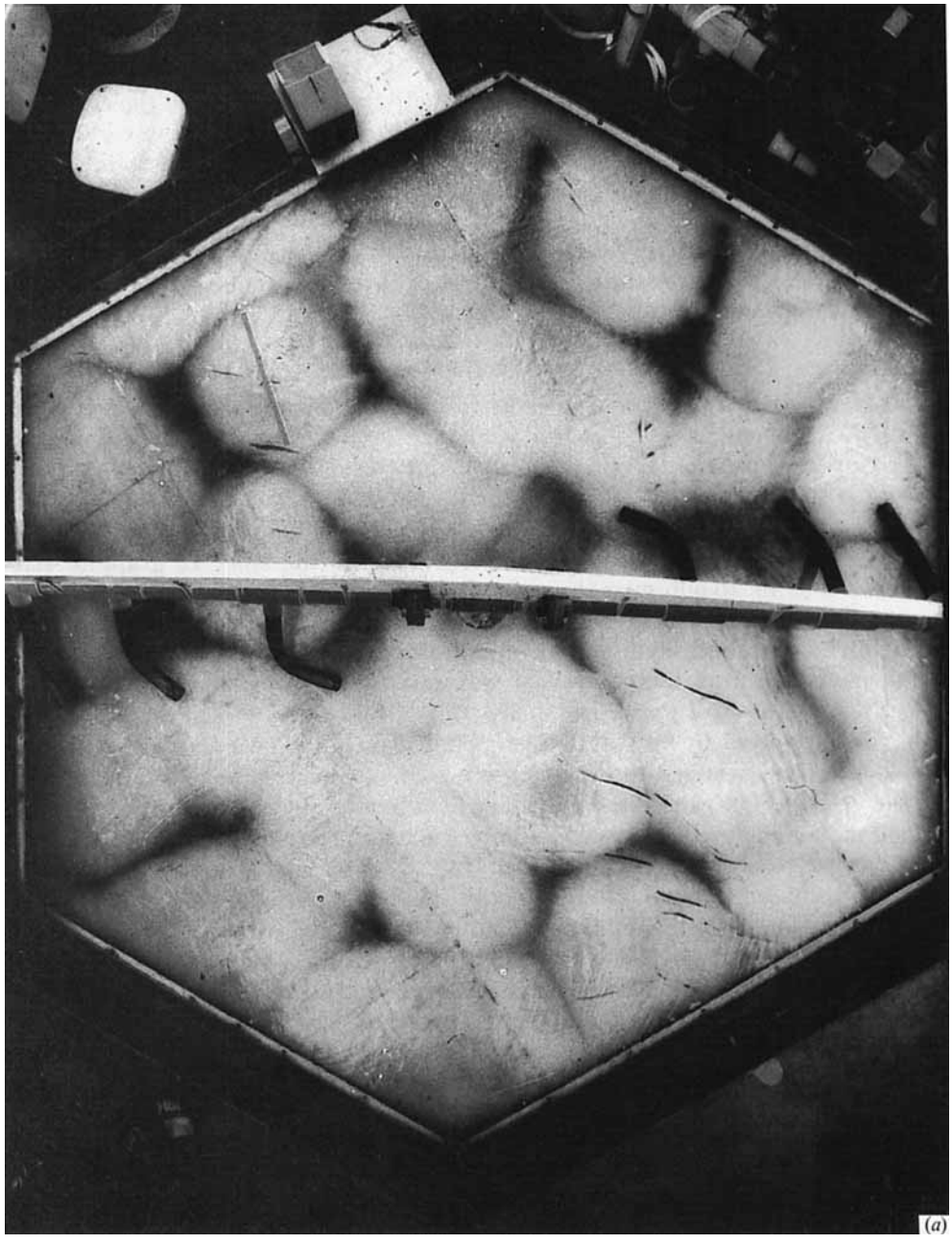

FIGURE 10(*a*). For caption see p. 304.

the other was slowly heated, and the shape of the apparatus could both be involved in the primary appearance of hexagons. The experiment with the semi-open top boundary also developed hexagonal patterns, but these were spaced 3.3 times the layer depth apart (Bories & Thirriot 1969). The larger scale confirms the semi-open nature of that top boundary; the influence of surface-tension effects on scale and pattern is unknown.

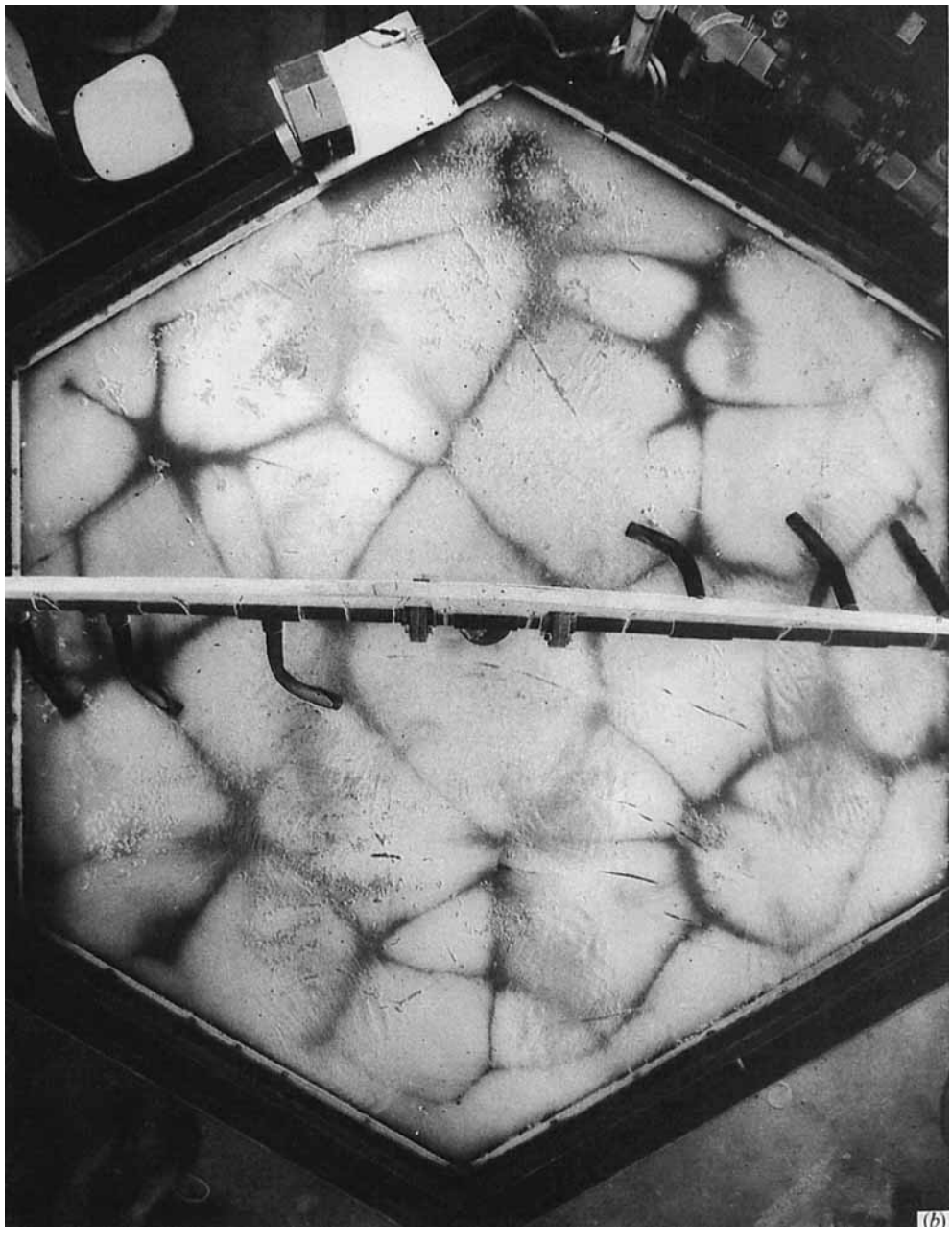

FIGURE 10(*b*). For caption see p. 304.

The first significant modification of the basic hexagonal pattern had developed by a Rayleigh number of 248, figure 10(*b*). This picture can be compared with the one obtained on the way down in Rayleigh number at 258, figure 10(*c*). The cold boundary temperature is colder and the power level is higher for the later picture, but the Nusselt number is similar and so is the pattern of convection, in character though not in detail. On the way up to figure 10(*b*) a significant event occurred which gives

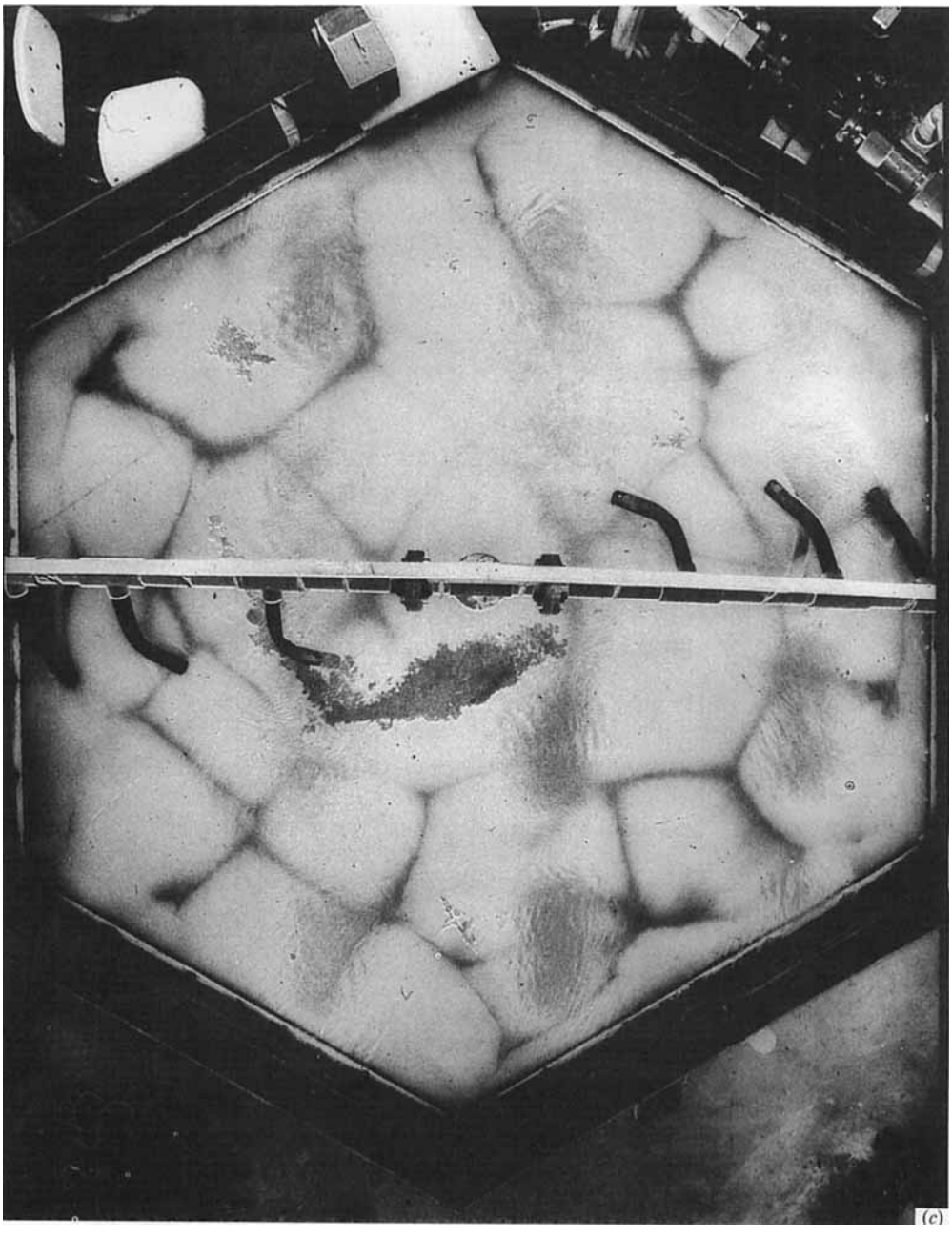

FIGURE 10. (*a*) Pattern of downwellings (dark) in the apparatus outlined by the collection of coloured liquid formed electrolytically at the top boundary. Photograph taken by a 35-mm camera fitted with a 17 mm wide-angle lens mounted near the ceiling near the centre of the apparatus. The image has been processed to remove the reflections of the room lights in the swirlpool above the cold boundary, utilizing the fact that the downwellings are blue, the background is yellow and the light reflections are white. A positive transparency taken through a green filter was sandwiched against a negative taken through a yellow filter to make the prints. Rayleigh number $\mathscr{A} = 50$ increasing, Nusselt number $N = 1.7$, power $W = 18$ W; corrected temperature difference $\Delta T' = 1.36$ °C; photo taken 305 min after the centre of a 10 min-long electrolytic pulse of 60 V at 2 A. A 47 cm-long rule is visible crossing an upwelling hexagon at top left. The very faint downwelling just below the mid-line is primarily due to a relative paucity of blue fluid manufactured there. (*b*). Pattern of

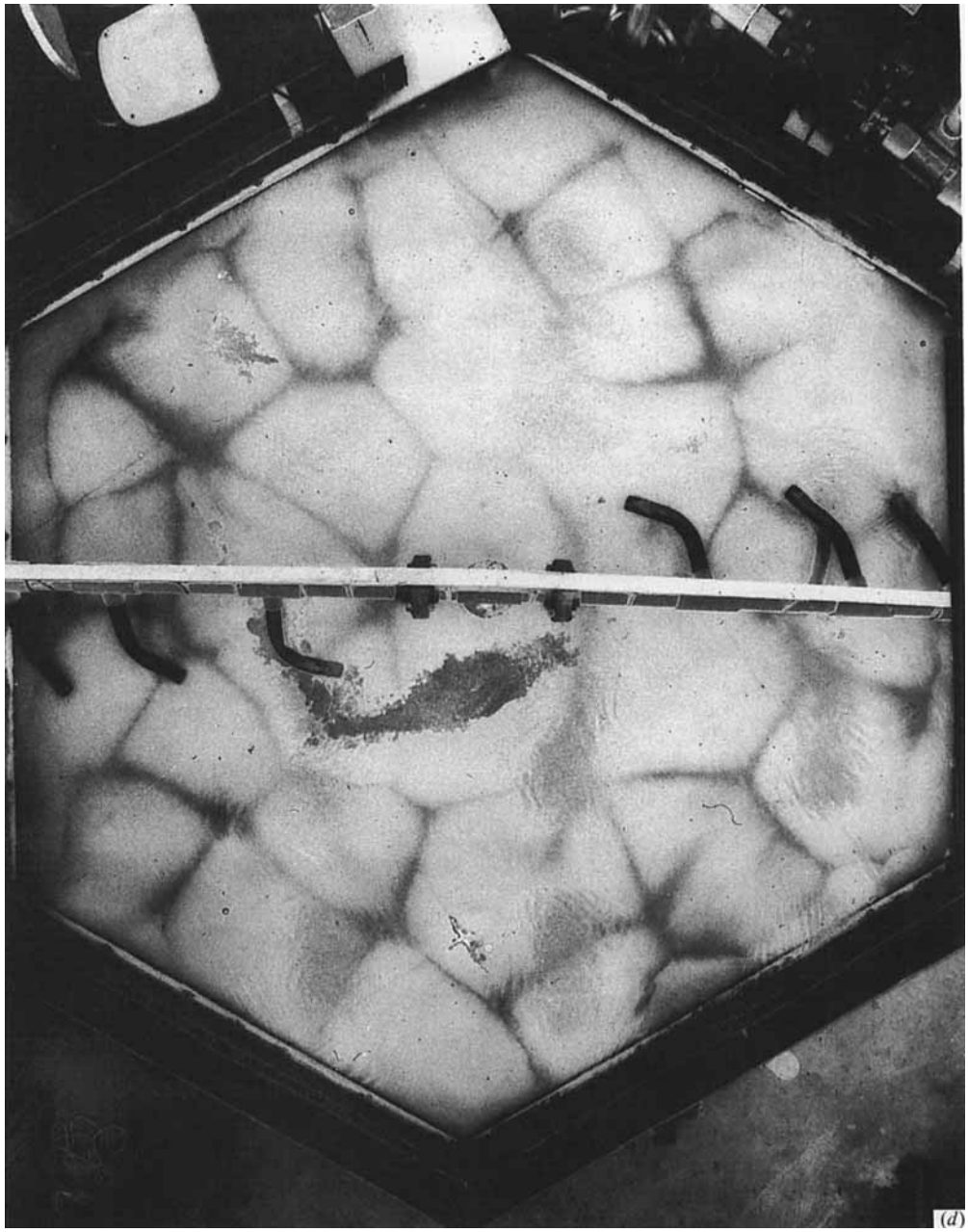

downwellings obtained as in (*a*). $\mathscr{A} = 248$ increasing, $N = 5.6$, $W = 248$ W, $\Delta T = 5.54$ °C, 33 min after colouring pulse, cold boundary 24 °C. The simple hexagonal pattern of (*a*) has evolved into a more complex one of interlinked downwellings. (*c*) Pattern of downwellings obtained as in (*a*). $\mathscr{A} = 258$ decreasing, $N = 5.7$, $W = 372$ W, $\Delta T = 8.45$ °C, 31 min after colouring pulse, cold boundary 16 °C. The pattern is qualitatively similar to (*b*), but different in detail. Fainter regions just above and below the cold water supply pipe (crossing the apparatus horizontally) are due to the non-uniform distribution of the graphite anodes. The irregular shape just below centre is a thin air bubble under the top film. (*d*) Pattern of downwellings obtained as in (*a*). $\mathscr{A} = 330$ *decreasing*, $N = 6.8$, $W = 545$ W, $\Delta T = 10.49$ °C, 15 min after colouring pulse. A clear family resemblance to (*c*), but there are more cells so that the pattern is smaller in scale.

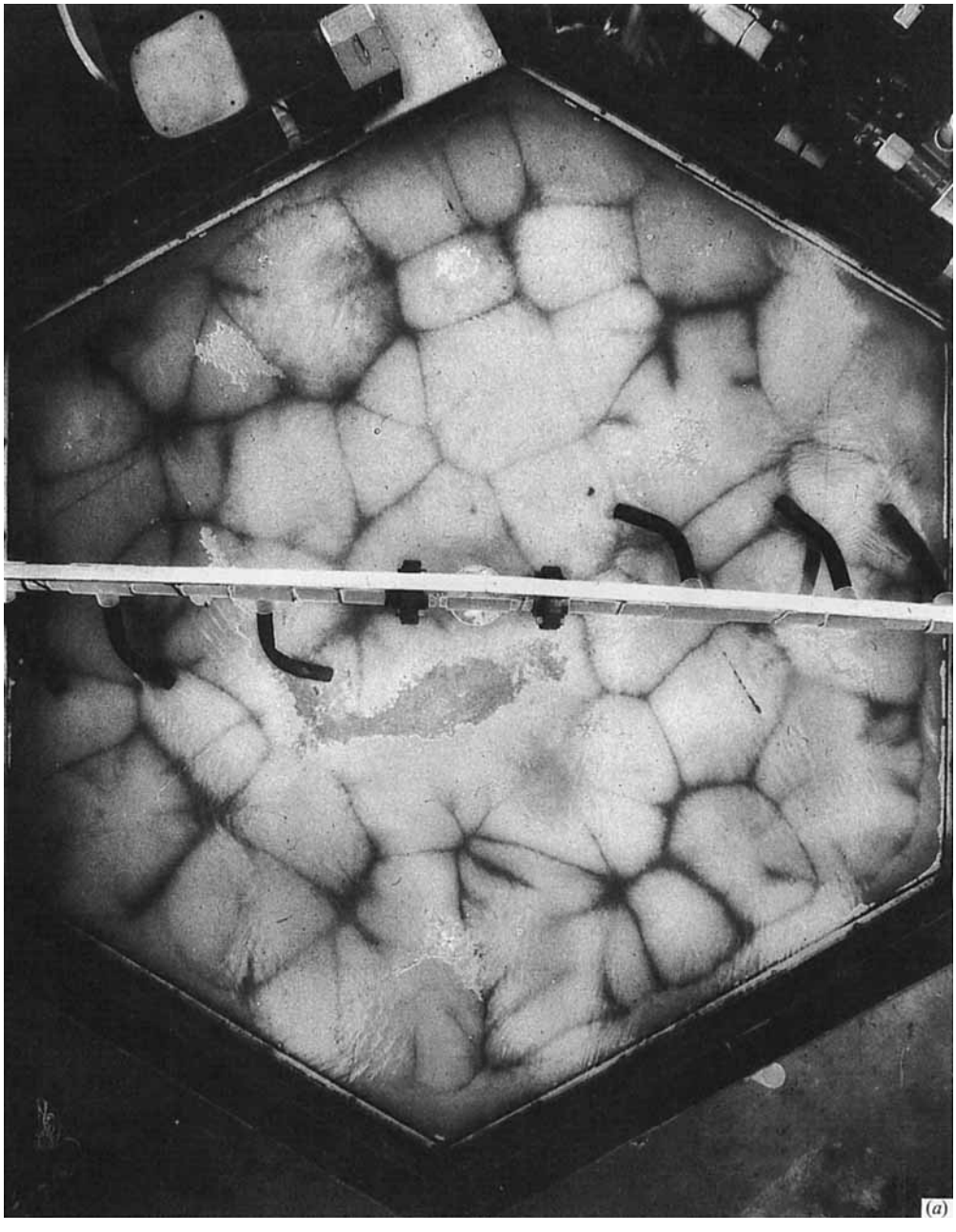

FIGURE 11 (*a*). For caption see p. 308.

insight into the mechanism of what is happening. The cold water supply failed and the circulator had to be shut down; owing to evaporation, this had the effect of cooling the cold boundary by 2.5 °C in 18 hr, more than doubling the temperature difference across the slab. The overall convection pattern was the same as in the previous normal image, but several of the flows toward downwellings had developed subsidiary, or tributary, downwellings at 90° to the main ones. The direction of the breakdown agrees with that of free convection in the presence of a large-scale shear

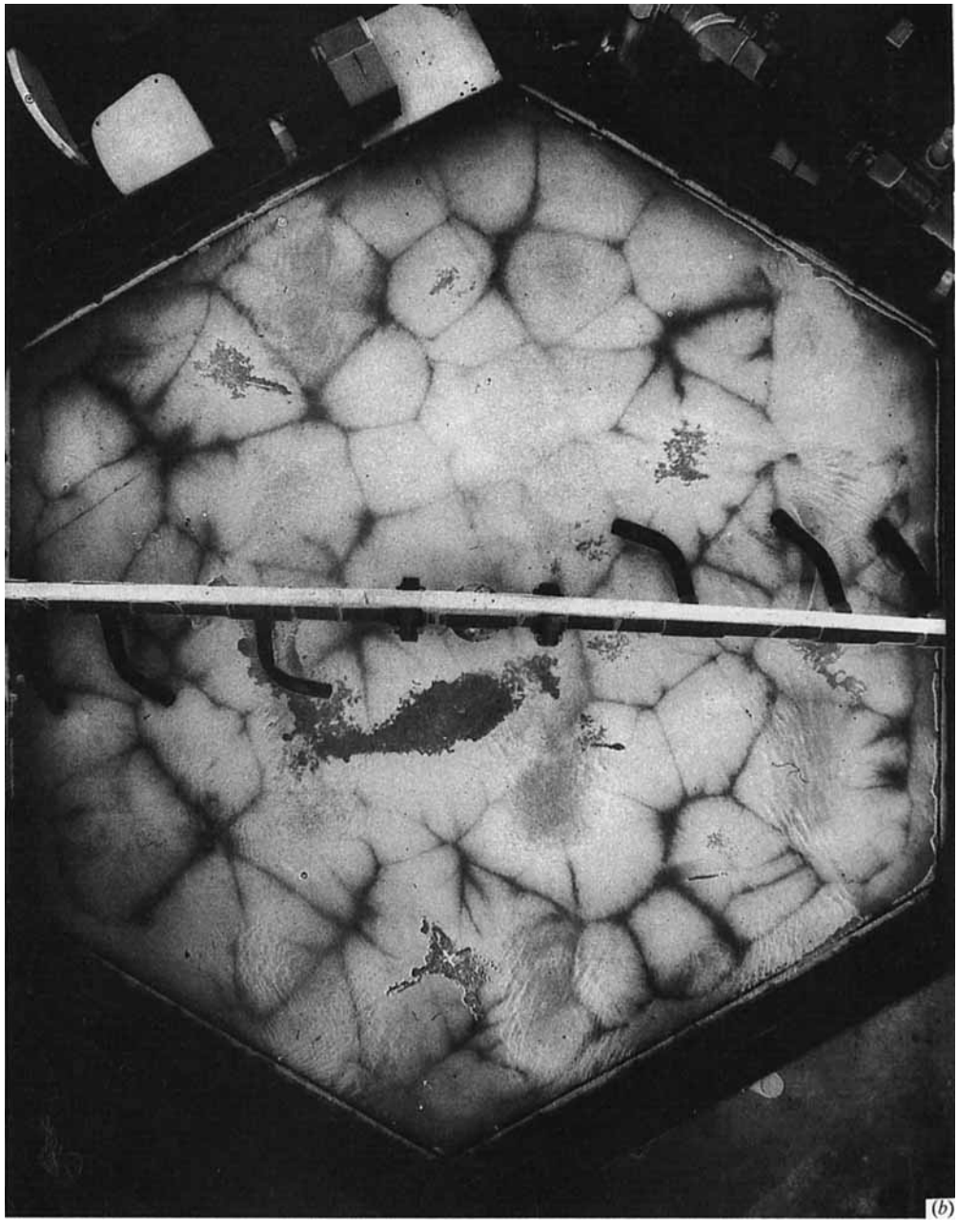

FIGURE 11(*b*). For caption see p. 308.

flow (Richter 1973), but the mechanism must be different, as the temperature drop across the boundary layer is not high enough for it to become unstable within itself. Two aspects are interesting: one is that exactly the same pattern restabilized after the 24-hr disturbance, even though the temperature difference between the boundaries dropped below critical for a while after circulation was restored; the other is that, given time for the pattern to re-equilibrate, it took almost another doubling of the temperature difference for similar features to appear. The temperature

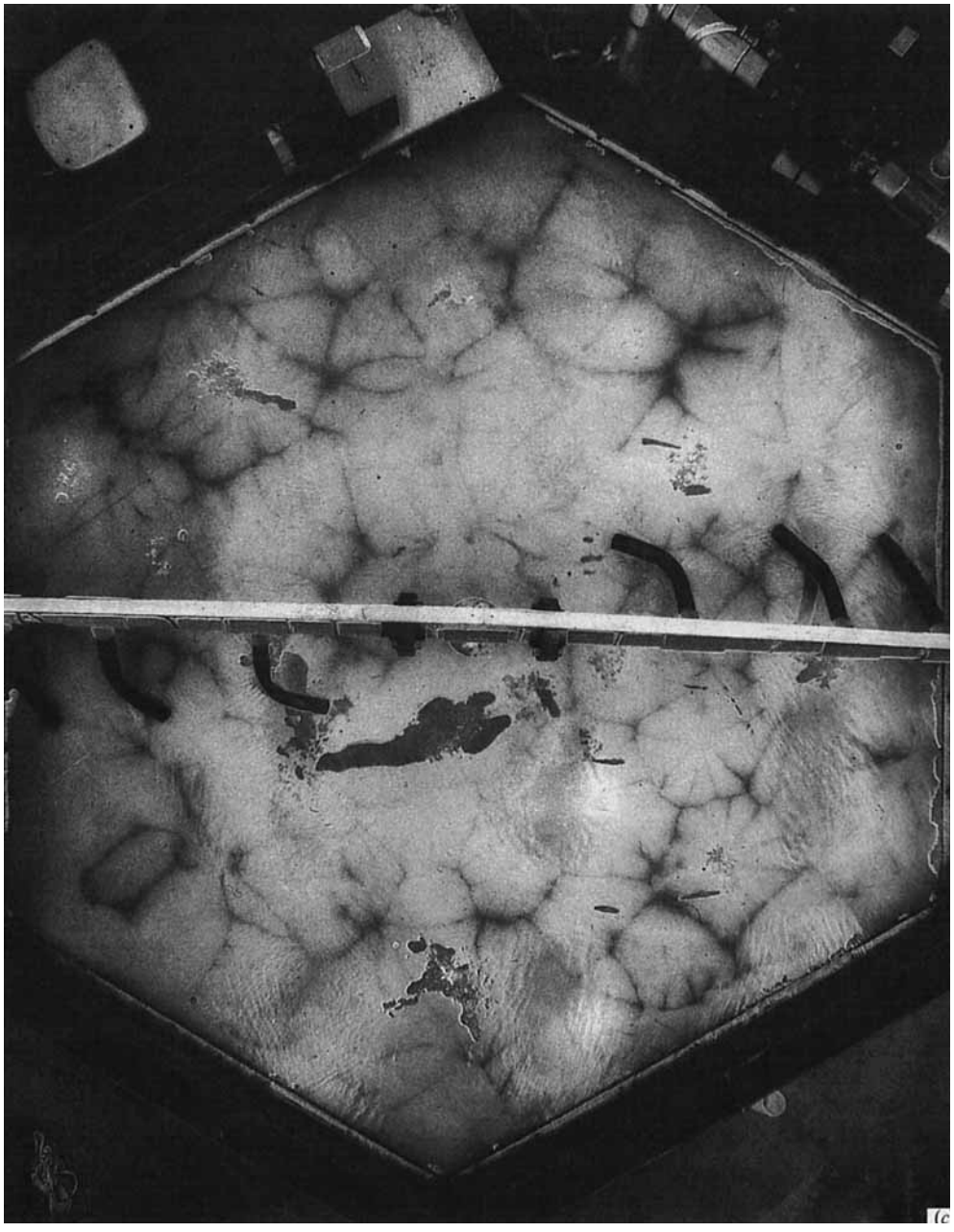

FIGURE 11. (*a*) Pattern of downwellings obtained as in figure 10(*a*). $\mathscr{A} = 576$ decreasing, $N = 1.1$, $W = 1212$ W, $\Delta T = 15.55$ °C, 12 min after colouring pulse. Still finer scale, and the beginning of a change in the number of downwellings that gather toward a node, or downwelling plume. (*b*) Pattern of downwellings obtained as in (*a*). $\mathscr{A} = 736$ decreasing, $N = 12.9$, $W = 1830$ W, $\Delta T = 18.35$ °C, 12 min after colouring pulse. Scale continues to shrink, and there is the beginning of a hierarchy to the downwellings. (*c*) Pattern of downwellings obtained as in (*a*). $\mathscr{A} = 1142$ decreasing, $N = 21.3$, $W = 4030$ W, $\Delta T = 21.22$ °C, 6 min after centre of colouring pulse with

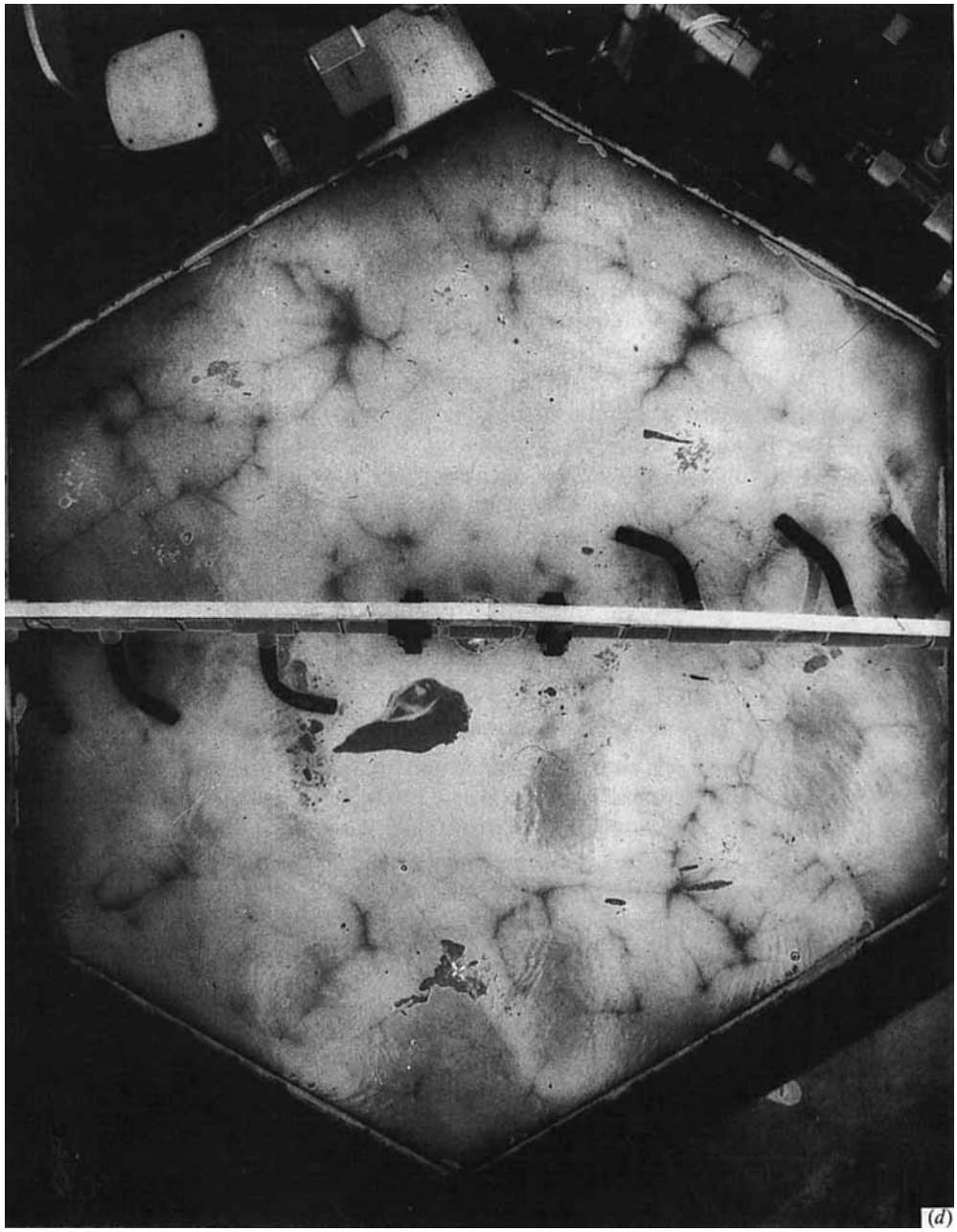

electrolysis still on. Blank areas have begun to appear where coloured liquid is not being produced as fast as it is swept away. A finer pattern and still more of a hierarchy to the downwellings. (*d*) Pattern of downwellings obtained as in (*a*). $\mathscr{A} = 1807$ decreasing, $N = 37$, $W = 9030$ W, $\Delta T = 24.37$ °C, 6 min after centre of colouring pulse with electrolysis still on. Dye production is now inadequate except directly over the 13 anodes, so that the pattern is incomplete, and the darkness observed has only a partial relation to the collecting area of the downwelling. In the few areas where similarity can be traced, the pattern seems to be substantially finer than in (*c*).

difference is now high enough for tributary convergences to develop on both boundaries, and, as the boundary flows are not independent, a very complex rearrangement of the pattern occurs. It is no longer a matter of hexagons trying to organize into rolls, but an intrinsically three-dimensional irregular pattern.

Figure 10(*d*) has an obvious family resemblance to figure 10(*c*), but some of the larger upwellings (blank areas) have been subdivided by downwellings to induce a finer general scale. A major change is apparent on figure 11(*a*), where tributary downwellings no longer exclusively act to subdivide upwelling zones, but begin to take on a dendritic aspect, feeding in toward foci, or major downwelling plumes. The increased sharpness of the picture is partly due to the visibility penetration depth, about 8 mm, becoming more comparable with the thickness of the boundary layer, 15 mm, at a Nusselt number of 10.

Figures 11(*b*)–11(*d*) show more of the same trend, not only to a finer scale, but to an increasingly dendritic plume-feeding structure. The thickness at which the boundary layer becomes unstable is shrinking more rapidly than is the horizontal spacing between plumes, allowing more complex feeding flows to develop. It is possible that, if the colour-generation scheme could have worked rapidly enough to give full coverage of the apparatus at the conditions of figure 11(*d*), another change in character might have been discernible. Where anodes were in upwellings, and allowed more than a single node to be made visible, there is evidence of a substantial decrease in the scale of the convective plumes. As will be discussed later, the boundary layer has shrunk to 4 mm, comparable in scale with the 3 mm bead size.

4.4. *Dependence of flow structure on Rayleigh number*

It would be useful to have some quantification of the change in pattern size with Rayleigh number, and yet this is very difficult because the pattern is not regular and it is hard to decide whether a faint downwelling trace does or does not subdivide a plume area. The results of two independent sets of observations are shown in figure 12. The linear fit would predict 60 plumes at the Rayleigh number of figure 11(*d*), while an estimate based on the changes in pattern size, where those can be followed between figures 11(*c*) and 11(*d*), is 72, not significantly different in view of the precision available.

4.5. *Heat transport*

The reliable measurements of Nusselt number are plotted against Rayleigh number in figure 13, again on the same scale as the prior data in figure 2. The curve outlined by the data is remarkably different from those of prior work. The onset of heat transport is very steep and rises above the theoretical 'upper bound' of Busse & Joseph (1972), the curve then flattens at a low Rayleigh number, but steepens to a slope of greater than 1 toward the highest Rayleigh numbers reached. One can argue that the equilibration times near the onset were inadequate, and that a data point such as the one labelled 'C' in figure 9, which was partially convecting, would have moved to a higher Nusselt number with a longer equilibration time. The triangles, obtained at decreasing power, do seem to be heading for a lower Rayleigh number of onset, but the data point labelled 'N', at a Rayleigh number of 27 was definitely not convecting: the heat leakage problem does not affect the temperature difference and the calculation of a Rayleigh number. The point obtained 16 days earlier (figure 9) shows traces of flow, a picture not very convincing either way, as if it was trying to die out. Thus, that Rayleigh number of 33 is a minimum for onset of convection, allowing for the very considerable lag time near the critical level. Shifting the scale

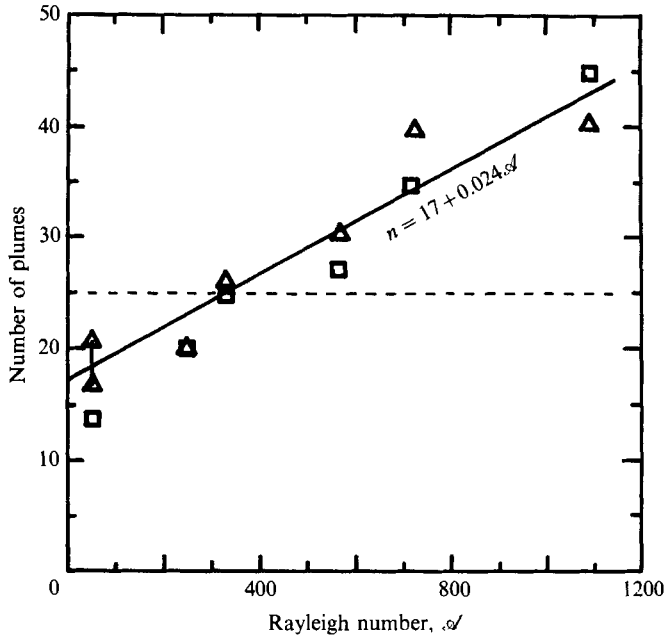

FIGURE 12. A plot of estimates of the number of upwelling plumes (blank areas) in figures 10(*a*, *b*, *d*), 11(*a*, *b*, *c*). Squares were obtained by Ling-Yun Chiao, choosing a 'typical' plume and dividing its area into that of the apparatus. Triangles were obtained by Lister by counting plumes on the tracings made by Chiao. The line is a 'reasonable' eyeball fit, not a true least-squares regression, allowing somewhat for the dashed line at 25. This is the number of times a hexagon two layer depths across the flats would fit into the apparatus area, if such a fit were geometrically possible.

so that 33 becomes $4\pi^2$ brings the points in the 50–80 Rayleigh-number range, below the Busse & Joseph (1972) bound, and makes the lower part of the new data follow curve 3 of Schneider (1963) obtained with 10 mm glass beads and turpentine. Splitting the difference between decay and onset, as would be the most appropriate reaction to the idea of time-delay hysteresis, leaves points well above prior data and slightly above the theoretical bound.

Even the most extreme readjustment of onset leaves a clear break in slope centred on a Rayleigh number of 80. The Nusselt number is about 3 and the convective pattern clearly defined and stable – hence the big gap between figures 10(*a*) and 10(*b*). The 24-hr cooling excursion discussed above gave the convective pattern an opportunity to change when it was near a Rayleigh number of 68, but it did not. The triangles in figure 13 retrace the same curve on cooling, and the analysis by stability of the boundary layer to subsidiary breakdown indicates that there should be no mechanism inducing change. One must conclude that the break in slope is an intrinsic property of the convection.

A five-week period of unchanging conditions separates the last filled circle on figure 13 from the first open circle. Air diffusion into the fill through the top membrane was beginning to precipitate near the hot boundary. At the highest thermal fluxes, flow was vigorous enough to force the bubbles to the surface, and it was then possible to bleed them from underneath the film. Some 5% by volume of air was eventually bled out, $\frac{1}{7}$ of the pore volume. Many more upwelling plumes developed in the open-circle region than under the corresponding conditions for the

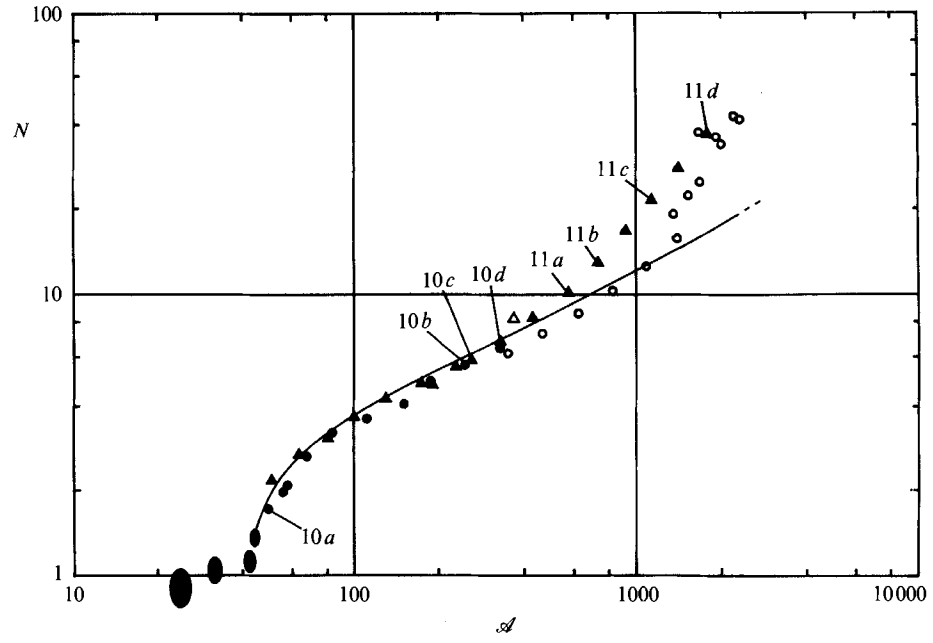

FIGURE 13. A plot of all the reliable Nusselt-number data against Rayleigh number, axes scaled using the results of figure 9. ●, Data obtained at steps of increasing power; ○ data clearly affected by the liberation and migration of air bubbles in the apparatus; ▲, main sequence at decreasing power steps; △ intermediate point taken 5 days after a final degassing excursion to full power, may not be adequately equilibrated. Numbers in circles relate points to the photographs of convection patterns at the cold boundary (figures 10 and 11). ——, Semi-theoretical curve obtained from a simplified treatment of boundary layers (see §5). Corrections applied are discussed in text.

triangles, as if blockade of the permeability near the hot boundary, where the air is least soluble in water, subdivided the plumes. Figures 10 and 11 were produced from photographs of circulation free of interstitially precipitated air, since, while interesting, the conditions of the open circles could not be reproduced. The implication for chemical precipitation in natural systems is that it should induce narrower convective cells than would otherwise occur, not the reverse as has been implied by many authors discussing various types of pipe convection models that are broader than they are high (e.g. Elder 1965).

The smooth sequence of triangles in figure 13, joining with the filled circles from the upward power sequence, can be considered a representative set of consistent experimental data, unaffected by major extraneous events or trends. Since many of the corrections applied to the data become large at high power levels, their association with the upward trend of the curve should be discussed. At the conditions of figure 11 (*d*), the raw temperature difference between the circulators was 35.70 °C, and the correction applied to account for boundary-layer drops, arising out of figures 5 and 8, was 4.21 °C. Had it not been applied, the Nusselt number would have been 12% lower and the Rayleigh number 12% higher. The temperature measured by S2 in the middle of the fill was 27.63 °C, while the effective mean temperature $T_{MC} = 0.5 \times (T_{HC} + T_{CB} - 0.4\mathscr{T})$ (3.4) was 34.04 °C. The first of these, being representative of the mean state of water in the porous slab, was used to obtain a corrected value of ν/κ, since the hot plumes are narrower than the cold plumes when their viscosity is much

less, and the measured average temperature of the fill is a better guide to the effective viscosity and conductivity than the mean temperature of the boundaries. However, the buoyancy of those hot plumes is the result of expansion of the liquid over the entire temperature difference across the fill, and so the mean temperature should be used, applied to a formula representative of the total expansion from 20 °C to $(2\,T_{MC}-20)$ °C, a simple and consistent version of the approximate effective boundary temperatures. In fact, whenever the hot boundary temperature was greater than 30 °C, the simple form of ACOR (3.3) used in (4.2) was replaced by

$$\mathrm{BCOR} = (1+(T_{S2}-20)\,0.0217+(T_{S2}-20)^2\,0.000062)\,(1+(T_{MC}-20)\,0.045) \quad (4.4)$$

For the conditions of figure 11 (*d*) there are three possible ways to make the Rayleigh-number correction:

$$\mathrm{ACOR}\,(T_{S2}) = 1.58; \quad \mathrm{BCOR}\,(T_{S2},\,T_{MC}) = 1.91; \quad \mathrm{ACOR}\,(T_{MC}) = 2.11. \quad (4.5)$$

The first would put the figure 11 (*d*) point well to the left of where it is on figure 13, steepening the upper part of the curve to a ridiculous degree; the extreme correction, as was used for the first experiment to prepare figure 8, would move it 10% to the right. This would put that particular point onto the curve of figure 8, but it would not alter the decisively different form of the two curves. The upward trend at high Rayleigh number for this experiment is real, and it is either associated with the diminution of convective scale shown by figures 10 and 11 or other experimental effects.

5. Discussion

5.1. *A semi-empirical fit to the heat transport*

Since the basic goal of this research is to develop enough understanding of convection in a porous medium to be able to extrapolate sensibly to full-scale geothermal systems, then approaches intrinsically confined to low or moderate Rayleigh number are of little value, be they experimental or theoretical. The usual procedure is to conduct an experiment, or experiments, and then model the results in some way that increases understanding. For example, Ping Cheng (1978) compiles a selection of results, in a similar manner to figure 2, and superimposes a theoretical upper bound (Gupta & Joseph 1973), calculations based on the Galerkin method (Straus 1974) and a direct numerical solution (Combarnous & Bia 1971). These agree with the jump in Nusselt number just above critical and with each other to a Rayleigh number of about 70, but diverge thereafter, and terminate in validity at a Rayleigh number of about 300. Interestingly, this is where the visualization scheme shows the pattern of convection to change character, and where the Nusselt-number curve of the second experiment turns upward.

The availability of both pattern and heat transport data for the second experiment suggests that the first should be utilized in some way to predict the second. The method that will be used is a very simple application of the theory of heat flow into a boundary layer, since it is clear from the Introduction, as well as the photographs, that phenomena in the boundary layers dominate the convection at high Nusselt number. In a boundary layer formed entirely by cooling into the free surface of a lateral advection, such as in the formation of lithosphere from the Earth's mantle, the heat flow is proportional to $1/t^{\frac{1}{2}}$, where t is age from the time of divergence (*Davis* & Lister 1974; Lister 1977). The deviation from this simple law at the actual divergence extends out to very short times, and, in particular, the *average* heat flow

out to age t conforms very closely to twice that at the terminating age. In a porous medium with a solid conductive boundary, the flow in constrained to be parallel to the boundary between the point of impingement of a plume from the other side of the layer until the fluid peels off again to form the return plume. Friction is between the fluid and the matrix, not fluid and the boundary, so that the flow picture conforms very closely to the free boundary in free convection, there being no special velocity shear near the boundary. Provided that the geometry of the spreading plumes does not change radically (such as from rolls to squares with quite different flow properties), the boundary heat flux should be proportional to $1/\tau^{\frac{1}{2}}$ where τ is the residence time of the fluid in the boundary layer. The geometry condition is reasonably well satisfied by the sequence shown in figures 10 and 11, since the pattern shrinks without changing character except for the gradual development of dendritic downwellings at the highest Rayleigh numbers.

The next step is to presume that the lateral velocity in the boundary layer remains proportional to the vertical plume velocity, since the former has not been measured, but the latter has. Data obtained by dye-line generation in a Hele-Shaw cell (Hartline 1978) has been closely fitted by the relation

$$V^* = 1.31\,(\mathscr{A} - 4\pi^2)^{0.72}, \tag{5.1}$$

where V^* has been non-dimensionalized by dividing the real flux velocity (observed velocity × porosity × Poiseuille correction factor) by κ/h (Booker, J. R. & Hartline, B. K., unpublished manuscript 1981). It was found that the areal scale of the convection cells is inversely proportional to $(\mathscr{A} + C)$ where $C = 708$ (figure 12), so their linear scale is proportional to $(\mathscr{A} + C)^{-0.5}$. Thus the residence time of fluid in the boundary layer is proportional to the linear scale divided by the velocity

$$\tau \propto (\mathscr{A} + C)^{-0.5}(\mathscr{A} - 4\pi^2)^{-0.72}, \tag{5.2}$$

and the mean heat flux, or Nusselt number, is then given by

$$N = 0.159\,(\mathscr{A} + C)^{0.25}(\mathscr{A} - 4\pi^2)^{0.36}, \tag{5.3}$$

after fitting the level to the data at a Rayleigh number $\mathscr{A} = 300$. This equation is the solid curve in figure 13 and a remarkably good fit to the data in the range $50 < \mathscr{A} < 500$. It cannot be expected to work near the onset, where the plume divergences and convergences fill most of the space, and diverges from the data where the latter's slope breaks upward at a Nusselt number of 10.

5.2. *Heat transport divergence at high Rayleigh number*

One of the mechanisms that could cause an upward break in the Nusselt number slope is the packing anomaly for beads at a flat boundary (figure 14*a*). In the case of the second experiment, the beads have a much lower conductivity than the fluid, while the water has a conductivity twice that of the matrix as a whole. For something like a third of the bead diameter, or 1 mm, the conductivity is effectively doubled, so that the increment in heat transport can be estimated by thinning the boundary layer by 0.5 mm. For the conditions of figure 11 (*d*), $N = 35.5$ and the boundary layer is just over 4 mm thick, so the conductivity effect should increase the heat transport by 13%. Even allowing for some modest further increase due to the rise in permeability, this boundary phenomenon cannot explain the factor-of-two actual increase in Nusselt number above the theoretical curve of figure 13, which accurately represents the trend of the lower Rayleigh-number data, including the onset of

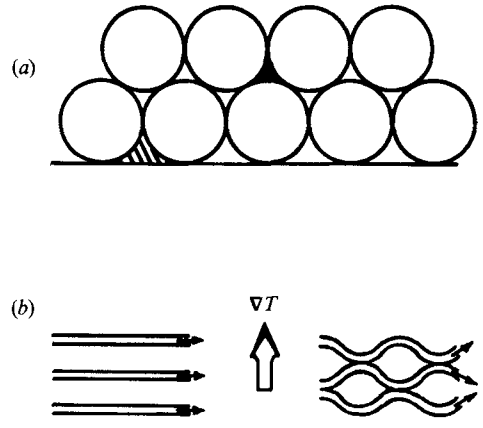

FIGURE 14. (*a*) A two-dimensional example of the boundary packing problem. Close packed cylinders have smaller spaces between them (black) than there are at the boundary (shaded). Conduction from the boundary begins entirely in the pore fluid. (*b*) Lateral thermal dispersion. Ideal flow in a porous medium is rectilinear (left). In a real bead medium, channels are tortuous and juxtapose flows from different levels in a transverse temperature gradient.

changes in the pattern. There was no such up-turn in the Nusselt-number curve for the experiment with fibrous fill (figure 8).

If it is a property of the fill that is causing the peculiar shape of the Nusselt-number curve, what property is it; in particular, what does the bead fill do that the rubberized fibre cannot? I propose that the key property is *lateral dispersion*. There is a fair amount of discussion in the literature about *longitudinal* dispersion, but, for thermal convection, longitudinal dispersion only adds some of the heat capacity of the fluid to that of the matrix. The thermal porosity is therefore smaller than the physical porosity, but the only known effect of the high thermal mass of the stationary matrix is to reduce or eliminate temporal changes in the pattern of convection. *Lateral* dispersion can, however, have a large effect on the convection when the boundary layers become comparable in size with the diffusion length of the lateral dispersion: the bead size. The pores between beads are interlacing channels, that is, they continually join and separate again, occasionally juxtaposing flows that would otherwise be separated by a substantial thermal-diffusion distance (figure 14*b*). Even without any turbulent mixing, this greatly enhances inter-channel thermal contact, and the use of beads with an irregular shape means that there will be some actual flow exchange between channels. Thus is the effective thermal diffusivity raised, but only if the flow velocity is sufficient to juxtapose channel streamlines more frequently than they would diffuse into equilibrium with each other by conduction. There is no effect from lateral thermal dispersion, either at the onset of convection or under conditions where the pores are fine enough to meet this new, more stringent requirement for 'true' porous-medium behaviour.

The heat transport measurements of the second experiment begin to deviate from the expected curve at a Rayleigh number of 400. Using the aforementioned measurements of plume velocity and the physical porosity of 0.38, the fluid velocity in the plumes should be about 0.23 mm/s, and the flow time around a bead should be about 20 s. The thermal diffusion time between flows that are on average 2 mm apart is about 60 s. The plumes are thus already subject to substantial lateral dispersion, and the more slowly moving horizontal boundary layers could begin to be affected. Unfortunately there do not seem to be any data on the lateral velocities of

boundary layers. In one reversed-polarity dye-line photograph of Hartline (1978), plumes are outlined by colour generation near the boundaries, and are narrowest $\frac{1}{4}$ to $\frac{1}{3}$ of the way across the Hele-Shaw apparatus. They gather flow from a base area of modest width and then mushroom toward the opposite boundary, suggesting that pressure and suction from the plumes is the primary drive, and that the velocity ratio is at least 3:1.

Lateral dispersion of the plumes could explain a phenomenon observed when the apparatus was freshly filled and contained regions of clear water, yellow bromothymol and blue bromothymol. The heater was turned on to mix the fluid, and, in spite of a very rapid rise in the temperature of the hot boundary, only large, featureless, single plumes were seen to appear at the top boundary, separated by 1.5 layer thicknesses. Mixing turned out to be very slow on the scale of the apparatus, since steady convection cells have closed streamlines: without some lateral dispersion it could have taken years!

5.3. *Quantitative differences between the experiments*

The remaining problem is the great difference in the position of the first breakover in slope of the Nusselt-number curves from the two experiments. In the curled fibre it is at $\mathscr{A} = 700$, $N = 22$, $\Delta T = 0.73$ °C, while in the polymethylmethacrylate beads it is at $\mathscr{A} = 85$, $N = 3.2$, $\Delta T = 2.02$ °C. The slopes of the post-break curves are not very different: 0.59 for the fibre and 0.52 for the beads, although by a Rayleigh number of 2580 the former is in a 'fluctuating regime' of some sort, while there is no evidence for any fluctuation in the bead experiment. There are no measurements, in part because the strong family resemblance between patterns from one sequence, taken weeks apart, seemed at the time conclusive evidence of flow stability. There might be pulsations in the flow rate, but the convection is not 'turbulent' in the free convection sense of an irregularly changing and non-repeating pattern. The form of equation (5.3) leaves limited options for the attainment of higher Nusselt numbers. The plume velocity simply cannot increase more rapidly than the Rayleigh number because the parameter kernel that determines the highest possible plume velocity, $\alpha \Delta T g D/\nu$, contains the only parameters that change significantly with Rayleigh number, and in the same relationship used in its calculation.

Neither the Hele-Shaw apparatus, in which the velocity measurements were made, nor the curled fibre medium, have significant lateral dispersion, but let us suppose that the corrections for colour diffusion in Poiseuille flow were in error and the power law obtained for velocity (5.1) is fortuitously correct only for the bead medium *with* dispersion. Then one can use an expression like $(\mathscr{A}^2 - 16\pi^4)^{0.5}$ for velocity in the curled fibre that tends rapidly to a linear relation with Rayleigh number. To obtain a linear relationship between N and $\mathscr{A}$ out of (5.3) still requires that the linear scale of the convection cells be proportional to $(\mathscr{A} + C)^{-1}$, a much more rapid change than found for the bead medium, and becoming significant much earlier (smaller C). For example, the equation

$$N = 0.02474\,(\mathscr{A} + 10)^{0.5}\,(\mathscr{A}^2 - 16\pi^4)^{0.25}, \tag{5.4}$$

obtained by the same square-root law of flux argument as (5.3) and fitted to the point $N = 10$ at $\mathscr{A} = 400$, provides a reasonable fit to the lower section of the data curve. Since there was no visualization in the first experiment, the pattern-related term $(\mathscr{A} + 10)^{0.5}$ must be considered pure speculation, and it is also a feature of experiments designed to reach very high Rayleigh numbers that data is poor near the onset. Had the apparatus been made of more corrosion-resistant materials, there

would be a case to be made for repeating the first experiment with a less permeable open-cell foam and the full visualization equipment. The lack of stabilizing thermal mass in the matrix may lead to a very different development of the convection pattern.

6. Conclusions

The solution of the geothermal problem of what the heat transport of porous-medium convection becomes at high Rayleigh number, hinges on the development of the boundary-layer structure and the spacing of plumes. For example, a theoretical treatment of free convection between fixed boundaries under conditions of very high Prandtl number (Roberts 1979) gave a basic relationship $N = f^{*0.2}$ where the factor f is a function of the aspect ratios of the cells. This function is not a simple power law, but close to a square-root relation when width/height is in the range 0.3–1. It is equivalent to the pattern-scale factor $(\mathscr{A} + C)^x$ in the Nusselt-number equations (5.3) and (5.4). Other work on the heat transport of two-dimensional flow over a heated strip indicated that the power law for a free boundary should have an exponent of 0.33 rather than the 0.2 of a fixed boundary (Roberts 1977). Applying the simple 'residence time' analysis of this paper leads to a flow velocity following a power law of $\mathscr{A}^{0.67}$, lending a little credence to the plume-velocity relation used in (5.3). While the view that boundary heat flux is inversely proportional to the square root of residence time in the boundary layer seems crude when compared to elegant mathematical theories, it offers the possibility of order-of-magnitude validity over a range of conditions beyond where those theories break down.

The first experiment, using a curled fibre medium, demonstrates that an upper-limit equation like (5.4) ceases to have validity well before free convection conditions take over in the apparatus. Even in the most compliant medium, boundary-layer subdivision cannot continue indefinitely at such a rapid rate, and the idea of Elder (1967) that $N \propto \mathscr{A}$ until free convection intervenes is not valid. Exactly what regime takes over is not established by the experiment, except that it includes fluctuations in temperature at a fixed measurement point. Since a medium of near 100 % porosity does not occur in nature, the further investigation of this problem cannot be given a high priority: the example has made its point.

The second experiment offers a solution to the problem of scatter in the results from prior experiments conducted in beds of beads of various kinds. Even under fully laminar flow conditions, lateral thermal dispersion increases the heat flux when the time for flow around a bead in a channel becomes comparable with the diffusion time across the bead. This effect is strongest when the beads are less thermally conductive than the fluid, and is minor when the reverse is true, such as with metal beads and oil. The extraordinarily high apparent Nusselt numbers obtained by Elder (1967) are probably due to the extreme contrast between the thermal conductivities of water and of polystyrene foam. Some of the remaining discrepancies may be due to differences in the methods used to correct for variations in fluid properties over the temperature ranges applied to the porous beds, since these methods are rarely reported.

The boundary flow visualizations over a wide range of Rayleigh numbers demonstrate two things: one is that, at Rayleigh numbers over 170, the convection becomes intrinsically three-dimensional, and cannot be properly modelled by either two-dimensional computational arrays or two-dimensional experiments, such as those using Hele-Shaw cells (Hele-Shaw 1898). The other is that the scale of the

convection *does* start to decline with increasing Rayleigh number, varying approximately as the inverse square-root of that number. If the peak plume velocity were proportional to Rayleigh number, which is the highest it can be in vigorous convection, then such a scale variation would be sustainable to indefinitely high Rayleigh numbers. This is because the time required for inter-plume thermal diffusion, changing as the inverse square of plume separation, would remain in constant proportion to the transit time of fluid in the plumes. If the plume velocity does not increase as rapidly as Rayleigh number, then the scale variation would enter a new regime where it would be limited by inter-plume diffusion, and the log-Nusselt-number curve would change from the slope of 0.61 predicted by (5.3) to 0.54, if the relation found by Hartline (1978) remained valid.

If the slope of the log-Nusselt-number/Rayleigh-number curve seems closely constrained to the 0.5–0.6 range, the level at which this slope is established remains more open. The breakover occurred at $N = 3$ in the layer of beads but at $N = 22$ in the bed of curled fibre, passing the Rayleigh number of 1000 at $N = 12$ and $N = 29$, respectively. The probability is that a low-porosity, low-dispersion medium, such as a cracked rock, would fall somewhere in the middle, such as passing $\mathscr{A} = 1000$ at $N = 19$. Thus the best prediction one can make for geophysical systems is

$$N = 0.425(\pm 40\,\%)\,\mathscr{A}^{0.55\pm 0.05} \tag{6.1}$$

at high Rayleigh number. This power law is between those predicted by the boundary-layer theories of Palm, Weber & Kvernvold (1972) and Robinson & O'Sullivan (1976). It requires a Rayleigh number of 93000 for the Wairakei geothermal area discussed in the Introduction. The plume separation, as a function of the equivalent layer scale height h, should be

$$S = 48\,(\mathscr{A} + 708)^{-0.5} h, \tag{6.2}$$

with unpredictable error bounds. The key feature is that the lateral scale of a convection cell is never greater than the layer height and decreases with increasing vigour of the convection. Geothermal plumes are therefore unlikely to be able to concentrate heat from a wide and diffuse source area. The effect of a precipitate that blocks channels near the hot end of the convecting slab (air) was found to greatly decrease the scale of the convection cells and only modestly depress the heat transport (figure 13 and associated text).

Experiments using beads to form the porous medium will have to be designed much more stringently in the future, to take account of lateral thermal dispersion. A medium approximating an array of vertical cracks would be much more representative of natural systems, has no boundary problems and no lateral dispersion, but poses formidable constructional difficulties, especially for large aspect ratios of the apparatus. Good measurements of plume velocity and the flow speed in the boundary layers would greatly improve understanding of the convective mechanism and could probably tighten the error bounds on the prediction of heat transport at high Rayleigh number.

This research was supported by National Science Foundation grants EAR77-23222, EAR83-16639 and OCE87-10059. Special thanks are due to Kenneth Gibson, a Master's degree student who contributed an exceptional level of effort toward the construction of the apparatus. Technician Randolph Fabro and colleague John Booker also provided significant help.

REFERENCES

BAKER, D. J. 1966 A technique for the precise measurement of small fluid velocities. *J. Fluid Mech.* **26**, 573–575.

BOOKER, J. R. 1976 Thermal convection with strongly temperature-dependent viscosity. *J. Fluid Mech.* **76**, 741–754.

BORIES, S. 1970 Sur les mécanismes fondamenteaux de la convection naturelle en milieu poreux. *Rev. Gen. Therm.* **108**, 1377–1401.

BORIES, S. A. & THIRRIOT, C. 1969 Echanges thermiques et tourbillons dans une couche poreuse horizontale. *Houille Blanche* **3**, 237–245.

BURETTA, R. J. & BERMAN, A. S. 1976 Convective heat transfer in a liquid-saturated porous layer. *Trans. ASME* E: *J. Appl. Mech.* **43**, 249–253.

BUSSE, F. & JOSEPH, D. D. 1972 Bounds for heat transport in a porous layer. *J. Fluid Mech.* **54**, 521–543.

CALTAGIRONE, J. P., CLOUPEAU, M. & COMBARNOUS, M. A. 1971 Convection naturelle fluctuante dans une couche poreuse horizontale. *C. R. Hebd. Séanc. Acad. Sci. Paris* B, 833–836.

COMBARNOUS, M. 1970 Convection naturelle et convection mixte dans une couche poreuse horizontale. *Rev. Gen. Therm.* **108**, 1355–1375.

COMBARNOUS, M. A. & BIA, P. 1971 Combined free and forced convection in porous media. *Soc. Petrol. Engng J.* **4**, 399–405.

COMBARNOUS, M. & BORIES, S. 1974 Modélisation de la convection naturelle au sein d'une couche poreuse horizontale à l'aide d'un coefficient de transfert solide-fluide. *Intl J. Heat Mass Transfer* **17**, 505–515.

COMBARNOUS, M. A. & BORIES, S. A. 1975 Hydrothermal convection in saturated porous media. In *Advances in Hydroscience*, vol. 10 (ed. V. T. Chow), pp. 231–307. Academic.

CORLISS, J., DYMOND, J., GORDON, L. I., EDMOND, J. M., HERZEN, R. P. VON, BALLARD, R. D., GREEN, K., WILLIAMS, D., BAINBRIDGE, A., CRANE, K. & VAN ANDEL, T. H. 1979 Submarine thermal springs on the Galapagos Rift. *Science* **203**, 1073–1083.

DARCY, H. P. G. 1856 *Les Fontaines Publiques de la Ville de Dijon.* Paris: Victor Dalmont.

DAVIS, E. E. & LISTER, C. R. B. 1974 Fundamentals of ridge-crest topography. *Earth Planet. Sci. Lett.* **21**, 405–413.

ELDER, J. W. 1965 Physical processes in geothermal areas. In *Terrestrial Heat Flow* (ed. W. H. K. Lee) Am. Geophys. U. Monog. no. 8, pp. 211–239.

ELDER, J. W. 1967 Steady free convection in a porous medium heated from below. *J. Fluid Mech.* **27**, 29–48.

FEHN, U. & CATHLES, L. M. 1979 Hydrothermal convection at slow-spreading mid-ocean ridges. *Tectonophys.* **55**, 239–260.

FISHER, R. G. 1964 Geothermal heat flow at Wairakei during 1958. *N. Z. J. Geol. Geophys.* **7**, 172–184.

GIBSON, K. M. 1980 The design and construction of an experiment to observe porous convection at high Rayleigh numbers. M.Sc. thesis, University of Washington, Seattle, WA.

GRINDLEY, G. W. & BROWNE, P. R. L. 1975 Structural and hydrological factors controlling the permeabilities of some hot-water geothermal fields. *Proc. 2nd UN Symp. on Development & Use of Geothermal Resources*, vol. 1, pp. 377–386. Washington, DC: US Govt. Print. Off.

GUPTA, V. P. & JOSEPH, D. D. 1973 Bounds for heat transport in a porous layer. *J. Fluid Mech.* **57**, 491–514.

HARTLINE, B. K. 1978 Topographic forcing of thermal convection in a Hele-Shaw cell model of a porous medium. Ph.D. thesis, University of Washington, Seattle, WA.

HARTLINE, B. K. & LISTER, C. R. B. 1977 Thermal convection in a Hele-Shaw cell. *J. Fluid Mech.* **79**, 379–389.

HARTLINE, B. K. & LISTER, C. R. B. 1981 Topographic forcing of supercritical convection in a porous medium such as the oceanic crust. *Earth Planet. Sci. Lett.* **55**, 75–86.

HELE-SHAW, H. S. J. 1898 *Trans. Inst. Naval Archit.* **40**, 21.

HOWARD, L. N. 1966 Convection at high Rayleigh number. *Proc. 11th Intl Cong. Appl. Mech.*, Munich 1964 (ed. H. Gortier), pp. 1109–1115.

KATSAROS, K. B., LIU, W. T., BUSINGER, J. A. & TILLMAN, J. E. 1977 Heat transport and thermal structure in the interfacial boundary layer measured in an open tank of water in turbulent free convection. *J. Fluid Mech.* **83**, 311–335.

KHURANA, A. 1988 Rayleigh–Bénard experiment probes transition from chaos to turbulence. *Phys. Today* **41** (6), 17–21.

KRISHNAMURTI, R. 1970*a* On the transition to turbulent convection. Part 1. The transition from two- to three-dimensional flow. *J. Fluid Mech.* **42**, 295–308.

KRISHNAMURTI, R. 1970*b* On the transition to turbulent convection. Part 2. The transition to time-dependent flow. *J. Fluid Mech.* **42**, 309–321.

LAPWOOD, E. R. 1948 Convection of a fluid in a porous medium. *Proc. Camb. Phil. Soc.* **44**, 508–521.

LISTER, C. R. B. 1974 On the penetration of water into hot rock. *Geophys. J. R. Astron. Soc.* **39**, 465–509.

LISTER, C. R. B. 1977 Estimators for heat flow and deep rock properties based on boundary-layer theory. *Tectonophys.* **37**, 157–171.

LISTER, C. R. B. 1984 The basic physics of water penetration into hot rock. In *Hydrothermal Processes at Seafloor Spreading Centers, NATO Adv. Res. Inst.* (ed. P. A. Rona, K. Bostrom, K. Smith & L. Laubier). Plenum, New York.

PALM, E., WEBER, J. E. & KVERNVOLD, O. 1972 On steady convection in a porous medium. *J. Fluid Mech.* **54**, 153–161.

PING CHENG, 1978 Heat transfer in geothermal systems. *Adv. Heat Transfer* **14**, 1–105.

RIBANDO, R. J., TORRANCE, K. E. & TURCOTTE, D. L. 1976 Numerical models for hydrothermal circulation in the oceanic crust. *J. Geophys. Res.* **81**, 3007–3012.

RICHTER, F. M. 1973 Convection and the large-scale circulation of the mantle. *J. Geophys. Res.* **78**, 8735–8745.

ROBERTS, G. O. 1977 Fast viscous convection. *Geophys. Astrophys. Fluid Dyn.* **8**, 197–233.

ROBERTS, G. O. 1979 Fast viscous Bénard convection. *Geophys. Astrophys. Fluid Dyn.* **12**, 235–272.

ROBINSON, J. L. & O'SULLIVAN, M. J. 1976 A boundary-layer model of flow in a porous medium at high Rayleigh number. *J. Fluid Mech.* **75**, 459–467.

ROSSBY, H. T. 1969 A study of Bénard convection with and without rotation. *J. Fluid Mech.* **36**, 309–335.

SCHEIDEGGER, A. E. 1974 *The Physics of Flow through Porous Media*, 3rd edn. University of Toronto Press, 353 pp.

SCHNEIDER, K. J. 1963 Investigation of the influence of free thermal convection on heat transfer through granular material. In *Porc. 11th Intl Cong. Refrig., Munich, Paper* 11-4, pp. 247–254.

SONDERGELD, C. H. & TURCOTTE, D. L. 1977 An experimental study of two-phase convection in a porous medium with applications to geological problems. *J. Geophys. Res.* **82**, 2045–2053.

STRAUS, J. M. 1974 Large-amplitude convection in porous media. *J. Fluid Mech.* **64**, 57–63.

STRAUS, J. M. & SCHUBERT, G. 1977 Thermal convection of water in a porous medium: effects of temperature- and pressure-dependent thermodynamic and transport properties. *J. Geophys. Res.* **82**, 325–333.

WARD, P. L. 1972 Microearthquakes: prospecting tool and possible hazard in the development of geothermal resources. *Geothermics* **1**, 3–12.

WOODING, R. A. 1957 Steady state free convection of a liquid in a saturated permeable medium. *J. Fluid Mech.* **2**, 273–285.